IEEE Access
Multidisciplinary | Rapid Review | Open Access Journal

Received 21 December 2022, accepted 16 January 2023, date of publication 25 January 2023, date of current version 30 January 2023.

Digital Object Identifier 10.1109/ACCESS.2023.3239782

TOPICAL REVIEW

A Review of 3D Printed Gradient Refractive Index Lens Antennas

IRINA MUNINA, (Member, IEEE), IGOR GRIGORIEV, (Member, IEEE), GARRET O'DONNELL, AND DANIEL TRIMBLE

Department of Mechanical, Manufacturing and Biomedical Engineering, Trinity College Dublin, Dublin 2, D02 PN40 Ireland

Corresponding author: Irina Munina (muninai@tcd.ie)

This work was supported in part by the European Union's Horizon 2020 Research and Innovation Program through the Marie Skłodowska-Curie under Grant 847402.

ABSTRACT Gradient index lens antennas find their application in modern wireless communication including radar systems, satellite communication, etc. They can ensure highly directional beamforming, support multibeam operations and beam steering capabilities within a wide angle of view. The development of 3D printing technologies enables the implementation of complex gradient refractive index distribution with high accuracy as well as obtaining a significant reduction in the production time and cost. This paper presents the state of the art in gradient refractive index lens antenna design using different types of additive manufacturing processes. It shows the applicability of 3D printing to a wide range of operational frequency bands from microwave to sub-THz and THz.

INDEX TERMS Additive manufacturing, antennas, 3D printing, radio frequency applications, dielectric lens, gradient refractive index lens, lens antennas.

I. INTRODUCTION

Nowadays, increasing data throughput and the rising number of users have led to new requirements for the hardware design for wireless communication networks, particularly antennas. Energy efficiency and low cost are not the only targets for antenna design. They should also provide broadband operation and agile control of the radiation pattern alongside low losses and low side lobes level. Simultaneously satisfying most of these requirements is the driving force for progress in antenna design and their fabrication processes.

Various types of antennas are used in modern wireless systems. For high frequency, especially millimetre-wave applications, antenna arrays or lens antennas can be used instead of single antennas in order to provide high directional properties and compensate path losses. For some applications, lens antennas can replace complex and expensive phased antenna arrays. Lens antennas can be used in radar systems, satellite communication, high data-rate wireless communication, and other systems. Through the design freedom offered by 3D printing the radiation pattern of the lens antenna can be customized for the intended application.

A lens antenna consisting of a dielectric body and antenna feed is shown in Fig. 1. Dielectric lens antennas are broadband, and the operational frequency range is often limited only by the bandwidth of the feed antenna. Dielectric lens antennas usually can be divided into two types: homogeneous

The associate editor coordinating the review of this manuscript and approving it for publication was Sandra Costanzo.

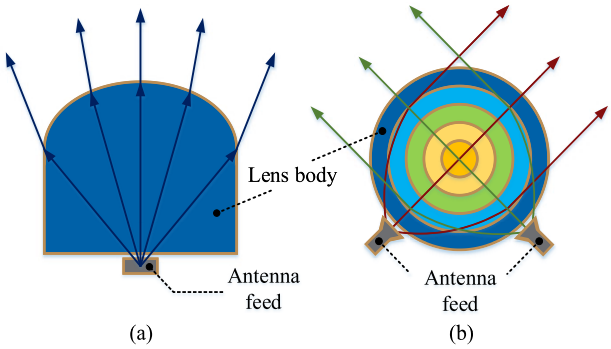

FIGURE 1. Homogeneous (a) and inhomogeneous (b) lens antennas.

lens antennas, in which the radiation pattern control is provided by the shape of the lens; and inhomogeneous (gradient refractive index - GRIN) lens antennas. In GRIN lenses, the wavefront transformation is provided by the gradient distribution of the refractive index along the lens profile.

Homogeneous lens antennas are characterized by highly directional properties. A radiation pattern of a given shape can be achieved by choosing a certain profile of the lens itself. The beam steering capability of homogeneous lens antennas is provided by placing several feed antennas on the lens surface and switching between them. This works for a limited field of view because the displacement of the feed antennas away from the focal point leads to a significant gain drop. In general, the fabrication of a homogeneous dielectric lens is simpler than an inhomogeneous dielectric lens, and the main goal during fabrication is to accurately reproduce the shape of the lens and its dimensions. Homogeneous lenses are highly dependent on the homogeneity of the dielectric material. Any anisotropy of the chosen dielectric material can cause internal reflections within the lens which leads to degradation of radiation performance.

Despite the above-mentioned drawbacks, these lenses can find niches for practical applications. The homogeneously integrated lens antenna was proposed for applications in unmanned aerial vehicles for high-speed, point-to-point communication with sensor nodes at 28 GHz [1]. The term ''integrated'' means that the feed is placed in direct contact with the lens body. For the E-band, the design of an integrated lens antenna with 2-D beam-steering capability within $\pm 4^\circ \times \pm 17^\circ$ and a maximum measured directivity of 36.7 dB was shown [2]. The design of a dome-shaped elliptical homogeneous lens antenna with the feed implemented as a ball grid array (BGA) was considered [3]. This antenna can be applied for high-data-rate backhaul/fronthaul systems for 5G communications. The homogeneous lens antennas with electronic beam control were considered promising for millimetre-wave backhaul applications [4], [6]. Additive technology can be also used for the design and fabrication of homogeneous lens antennas [7], [8].

The other extensive class of dielectric lens antennas is non-homogeneous, more often called gradient refractive index [9], [14]. The directional properties of such lenses are defined not only by the lens shape and size, but also by the refractive index distribution. Manipulation of refractive index distribution enables control of the radiation properties of these GRIN lenses. This helps to support not only high directional characteristics, but also provides low side-lobe level and wide-angle scanning. Until recently, the fabrication of GRIN lenses has been challenging. This involved complex structures consisting of several materials with different refractive indexes [15], [16]. In [16] a Luneburg lens design using the quasi-conformal transformation optics (QCTO) was designed and made from a set of polymer composites. The required refractive index gradient distribution was ensured by using combinations of materials with specific dielectric permittivity, and therefore the manufacturing process was complicated and time-consuming.

For some GRIN lens designs, it is possible to obtain the desired gradient index distribution by perforating solid dielectric materials [14], [17], [22]. Milling the air voids in solid dielectric materials changes the effective permittivity. This method requires the high accuracy associated with milling to achieve the pre-defined refractive index distribution [14], [21]. A GRIN lens based on a stack of dielectric sheets with perforated air voids was shown in [23]. The paper [24] described a passive frequency-coded retroreflective tag landmark based on a flattened perforated quasi-conformally transforming Luneburg optical lens. In the study [25], a perforated Luneburg lens was used to improve the radar cross-section (RCS) in the W-band.

GRIN lenses can also be implemented as fully metallic structures. The gradient refractive index distribution can be realised by varying the distance between metal plates or changing the height of the metal pins. By changing the height of pins and the period of their arrangement, the propagation constant inside the structure can be controlled. Such lenses are usually fabricated by subtractive methods. In [26], the design of a two-dimensional low-profile Luneburg lens was presented for satellite communication applications. The lens consists of two metal plates with periodic metal pins. An all-metal two-dimensional partial Maxwell fisheye (PMFE) and a planar reflective Luneburg (RLL) lenses were designed by using metal pins of variable height [27], [28]. Another type of lens antenna that uses a variable lens profile is the geodesic lens [29], [33]. In [34], a half geodesic Luneburg lens for Ka-band applications was considered. Due to the use of spline functions, it was possible to halve the size of a Luneburg lens and preserve the value of the realized gain.

Traditionally, the implementation of GRIN lenses was based on using natural materials with required dielectric properties or man-engineered materials with pre-defined effective parameters. Artificial materials can be realized by subtractive technologies such as the milling of metal or dielectric plates. These technologies can be time-consuming and can suffer from low accuracy. Significant progress in the fabrication of homogeneous and GRIN lens design has been made with the development of additive manufacturing (AM) technologies. It has led to the broadening of applications of lens antennas in wireless communication.

3D printing technologies have the potential to meet the design requirements for modern antennas. It enables the manufacturing of extremely complex geometric profiles with a significant reduction in production time and cost. While many 3D printing technologies are already characterized by high resolution, it is expected that resolution will continue to improve in AM technologies.

The process of antenna fabrication using AM can be divided into two steps. The first step is printing the part (Fig. 2). The wide variety of materials (dielectrics and metal) are available for 3D printing. For many types of antennas, the

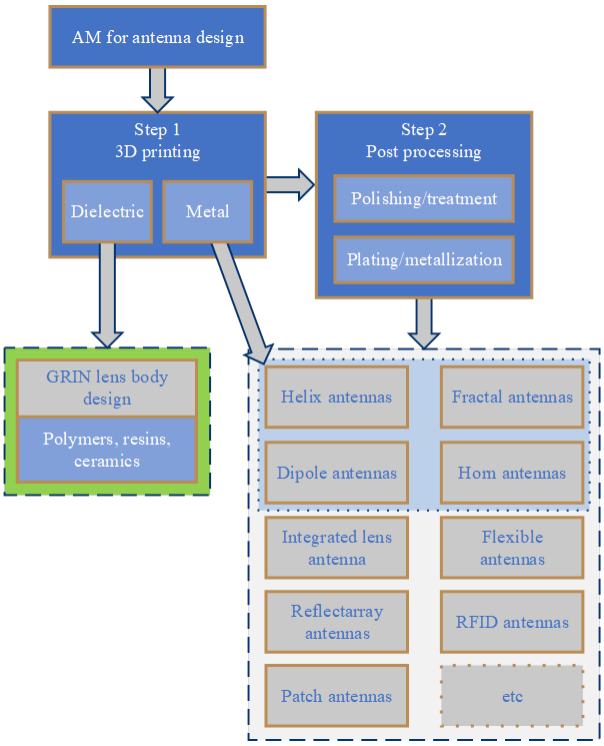

FIGURE 2. Additive manufacturing for antenna design.

second step is required. The second step can include post-processing as polishing or treatment of the surface of the printed part or/and plating/metal deposition. Postprocessing for example polishing can change the dimensions of the printed object. It is important to take it into account, especially for millimetre wave and terahertz applications.

The paper will focus on printing dielectric GRIN lens bodies using different printing technologies. AM gives freedom in the design of man-made materials with various effective electromagnetic parameters in a single manufacturing process. Based on these advancements, additive manufacturing is becoming a driver for rapid development of GRIN lens antennas, including the millimetre and submillimetre-wave applications.

This paper is organized as follows: in Section II an overview of 3D printing technologies which can be used for antenna design are considered, including the parameters and printing materials. In Section III, different GRIN lens designs utilising 3D printing technologies are shown. This section is subdivided by the different types of the 3D printing technologies used. The chosen examples covered a wide frequency range from microwave and millimetre wave to sub-THz and THz. In the last section, the advantages and drawbacks of additive manufacturing for GRIN lens antenna design are concluded.

II. ADDITIVE MANUFACTURING

At the end of the 20th century, the evolution of manufacturing processes led to the emergence of alternatives to traditional methods such as turning, milling, drilling, grinding, casting, etching, or other methods of mechanical or chemical processing. New ideas and principles of three-dimensional manufacturing by selectively adding 2D profiles, usually layer-by-layer emerged. The idea of rapid prototyping using AM started to be discussed in the early 1970s. Since then, AM has developed rapidly and become more affordable and therefore is no longer limited to professional use. The progress in AM continues today with the incremental improvement of existing technologies, and development of new technologies and improved material sets. To date, AM has applications not only in mechanical or bioengineering, but also in electronics and wireless communication systems. As such, the sole focus is no longer on the mechanical properties of 3D printed parts, but also on the electromagnetic properties of materials. The AM processes most commonly used for antenna design are fused deposition modelling (FDM), stereolithography (SLA), jet modelling (JM), and selective laser sintering (SLS).

A. FDM PRINTING

One of the most popular and affordable 3D printing technologies is Fused Deposition Modelling (FDM). The principle of FDM technology is the sequential deposition of molten thermoplastic in 2D layers to create a 3D part. (Fig. 3). This technology is also known as Fused Filament Fabrication (FFF). FDM/FFF is the most inexpensive 3D printing technology to date whereby both the cost of the printers and consumables can be very low. A wide variety of materials with different properties makes this technology one of the most versatile. It is also characterized by the high speed of printing. The drawback of FDM is poor surface roughness from the as-built state. However, this issue with surface roughness can be corrected by mechanical post-processing or chemical treatment. In addition, FDM printed parts can be used for both feature and form generation and then be followed with a plating step or coated by conductive materials. As FDM is quite commonly used for antenna prototyping, the reader can be referred to [35] and [38] for further details where printing was followed by a metallization process.

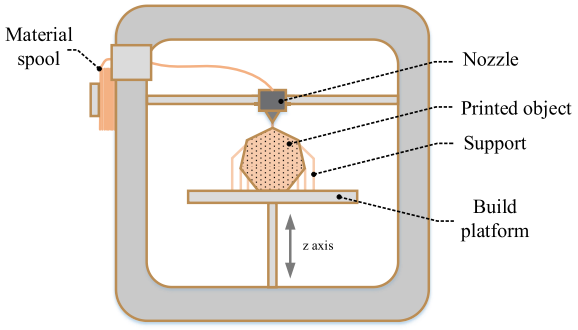

FIGURE 3. The Fused deposition modelling (FDM) process.

The efficiency of FDM prototyping of UHF antennas was shown in [39]where a broadband Yagi-Uda antenna

operating at 2.45 GHz was produced. In [40], the possibility of using FDM for printing a substrate for a microstrip patch antenna was studied. An FDM-printed X-band horn antenna was explored [35]. Comparing the characteristics of a printed antenna to an aluminium horn antenna of the same size showed a good agreement in performance, but the weight of a printed antenna was significantly less than the metal antenna demonstrating the impact of FDM printed antennas.

B. SLA PRINTING

One of the most popular AM technologies is stereolithography. The basic principles of SLA lie in the polymerization of photosensitive material under ultraviolet (UV) light. The peculiarity of this technology is the necessity for UV curing after printing to improve mechanical properties of the part such as the tensile strength and the ductility. The resin illumination process is based on vector or multiple laser scanning.

Depending on the position of the resin tank and UV source, two different types of SLA printers exist. The bottom-up SLA printer consists of a tank with a transparent bottom, which is filled with a liquid photopolymer; a vertically moving platform, on which the photopolymer hardens, and a source of UV light (Fig. 4). Such printers are mostly used for in-house applications. The industrial SLA printers are usually top-down (Fig. 5). They can support printing of bigger parts and ensure higher resolution in comparison with the bottom-up process.

Digital light processing (DLP) uses LED projection instead of laser systems as the UV source which reduces printing time (Fig. 6). The advantages of SLA and DLP are high resolution and a wide choice of materials. However, there is a trade-off between resolution and printing speed. The printing speed is also inextricably linked to model size and complexity. The resins for printing differ not only in mechanical properties but also in the resolution which can be achieved. For example, even the colour of the resin can affect the accuracy of the model whereby darker resins provide better resolution due to better light absorption. Because 3D printing is able to build a model in three directions, the resolution can be

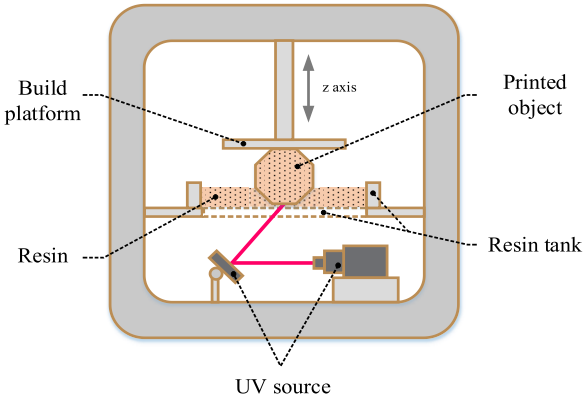

FIGURE 4. The bottom-up stereolithography (SLA) process.

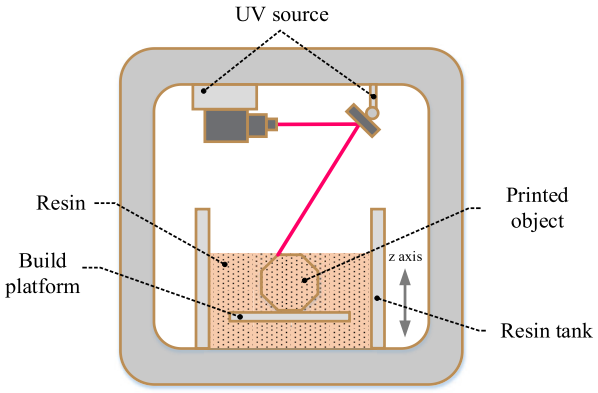

FIGURE 5. The top-down stereolithography (SLA) process.

defined for XY plane and Z direction. More often in specs, Z-resolution or layer height is referred to as a parameter that defines how fine can be features of the model. For RF applications, only Rogers Corporation provides RadixTM printable dielectric that has a dielectric constant $\varepsilon_r = 2.8$ and a dissipation factor $\tan\delta = 0.0043$ at 10 GHz, and $\varepsilon_r = 2.8$ and $\tan\delta = 0.0046$ at 24 GHz after curing [41]. The materials for photopolymer technologies are also offered by 3DCeram [42]. Carbon Digital Light Synthesis technology can potentially be used for the production of lens antennas. This is a resin-based 3D printing process that uses digital light projection. Carbon 3D provides epoxy-based material EPX82^{TM}. The mechanical properties of the material were described in detail [43]. However, information about the dielectric properties was only specified as $\varepsilon_r = 3.4$ and $\tan\delta = 0.007$, no frequency dependent behaviour was given. The loss tangent of EPX82TM is 1.5 times higher than Radix^{TM}. To date, Radix^{TM} is the only resin available on the market with dielectric properties industrially characterized over a wide frequency range (up to 24 GHz). The majority of the resins that are more widely available are not intended for antenna applications and therefore the dielectric properties must be characterised in-house.

SLA is capable of high-performance printing up to 10 microns resolution. For the majority of SLA printers resolution up to 25 microns can be achieved. One of the advantages of SLA is the low surface roughness of the printed parts. The photopolymer is used in liquid form and has a much higher wettability, which leads to smooth contact between the layers. The disadvantage of SLA is the high cost of consumables and the capital cost of the high-resolution printers.

There are some examples of antenna design fabricated using SLA [44], [46]. The design of broadband, dual-polarized, wide scan, phased array radiators operating at S-, X-, Ku-, and W-Band was shown in [46]. SLA has been shown to provide good feature resolution down to 100 microns for printed antennas. In [45], SLA was used to print MIMO antennas for 5G base stations. An antenna consisting of two orthogonal polarized dipoles was used for

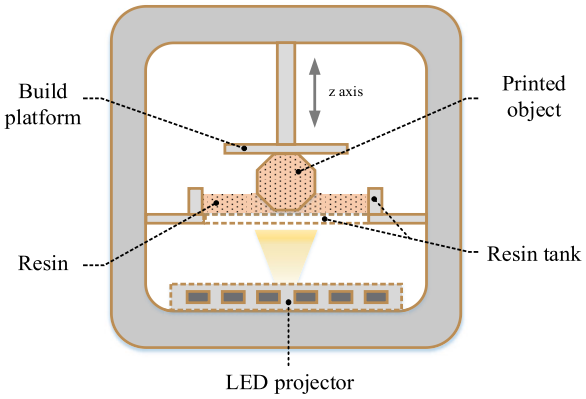

FIGURE 6. The digital light processing (DLP).

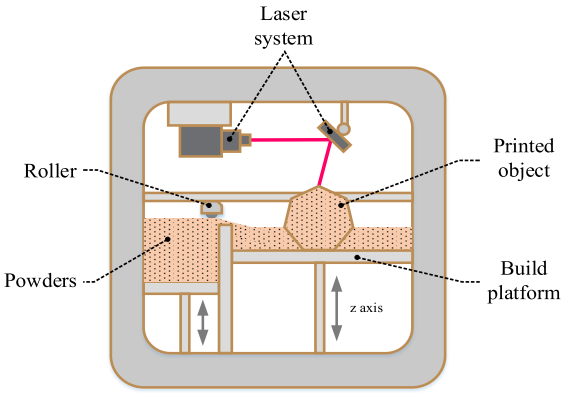

FIGURE 8. The Selective Laser Sintering (SLS) process.

this system. The antenna was printed from photosensitive resin and then metalized by copper plating postprocessing. In [44], the possibilities of using SLA/DLP for the fabrication of D-band slotted waveguides in combination with a chemical silver coating were investigated. A slotted spherical antenna operating at X- and Ku-bands was printed by using SLA and subsequently plated [47]. The antenna array based on glide-symmetric holey gap-waveguide manufactured with high precision SLA and subsequent metal plating was presented in [48].

C. JET MODELLING/MULTIJET PRINTING

Jet Modelling (JM) is based on the layer-by-layer curing of material under UV radiation. The technology enables the printing of waxes and photopolymer resins. The main features of this method are multi-jet printing, the variety of different materials and quality of a printed model. The printing head can contain up to several hundred nozzles which can be fed by various materials. After applying the material to the printed surface, a UV lamp is used for curing (Fig. 7). JM enables printing layer thickness of 15 microns. The main advantages are a smooth surface finish and high resolution of the printed parts. However, models can be vulnerable to direct sunlight which degrades their mechanical properties.

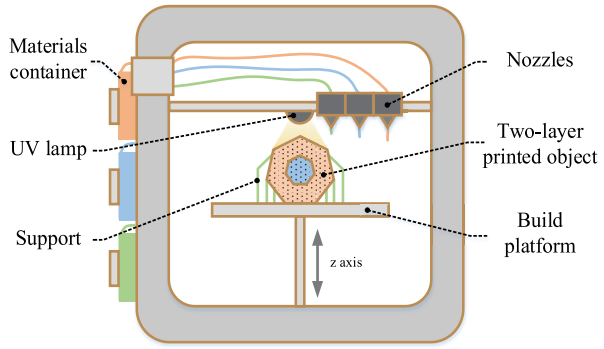

FIGURE 7. The Jet Modelling process.

HP Multi Jet Fusion technology is a JM process [49] that uses a high-speed synchronous architecture and builds parts layer-by-layer. It consists of a dual carriage scanning system with one carriage for recoating the area with fresh material and the other with functional agents. Hence, the processes can be separately optimized to ensure better performance, higher reliability, and productivity.

D. SLS/SLM PRINTING

Another type of AM process is Selective Laser Sintering (SLS). It is based on the selective sintering of loose powder by a laser. During the printing process, the powdered material is distributed over a platform using a roller, next, a laser selectively sinters the powder following a defined path (Fig. 8). For SLS, support structures are not required, even for extremely complex-shaped models. The powder itself is used as a support material. The technology is characterized by a wide variety of materials with different mechanical and electromagnetic properties. It is mainly used for the manufacture of parts from polymers or composites. This technology produces parts with good mechanical properties. However, the parts, in most cases, require post-processing due to roughness and porosity. The parts can suffer from poor roughness in comparison to SLA, which can limit SLS application to the millimetre and submillimetre-wave antenna design.

An SLS-printed K-band pyramidal horn antenna was studied in [50]. When compared with a traditional metal sample produced by casting, it was noted there was good agreement in antenna performance. A comparative study of flat-panel antennas for the millimetre-wave range fabricated by traditional subtractive manufacturing and SLS technology was shown in [51]. It was demonstrated that SLS offers more versatility for complicated designs which are difficult to fabricate by traditional milling processes, however, it was noted that surface roughness was poor. In [52] an SLS-printed circular array with electroplating was presented. It was designed for WiMAX base station applications.

In terms of the mechanical properties such as strength and ductility, traditional materials processed using machining

outperform SLS. However, parts manufacturing using Selective Laser Melting (SLM) can compete with those processed using machining. During the melting, the depth of the melting exceeds the thickness of the layer, which leads to remelting of the previous layer. The main difference between SLM and SLS is the laser system, whereby in the SLM process the melting temperature of the powder must be achieved. This means that the wavelength of the laser radiation must be compatible with the absorptivity of the powders. One of the main disadvantages of SLM is residual stresses in the printed part due to large heating and cooling cycles which can lead to part deformation and brittleness. Additional postprocessing for relieving the stress is necessary. The technology is commonly used for printing using conductive powders [53], [57].

Additive manufacturing includes more than 30 different technologies. In this section, the most popular technologies were considered and followed by the references. In the next section, the application of additive manufacturing to more complex RF challenges such as the developed of gradient refractive index lens antenna is examined in detail.

III. GRIN LENS DESIGN BASED ON 3D PRINTING

This section will be focused on 3D printing using dielectric materials for GRIN lens design. In comparison with [13], [16], and [22], additive technologies enable the production of lenses with a inhomogeneous refractive index distribution and a complex shape in a single fabrication process. It brings an additional degree of freedom to the lens design and allows to obtain the parts with man-engineered dielectric parameters.

A. FDM PRINTING FOR GRIN LENS DESIGN

FDM is a good starting AM technology due to the low cost of the printers and consumables. The FDM process are quite ubiquitous, the associated software is both easy to use and often open access. There is a wide range of available materials for FDM and some of these materials are already characterized for RF and microwave applications. With this level of openness and ease of use, FDM has been a rapid go-to technology for early-stage design. FDM is very often used for the GRIN lens implementation, mostly for microwave applications.

The required distribution of the permittivity inside the lens can be usually realized in two ways. The first approach is to recalculate the required permittivity into a percentage of plastic infill [58]. The second approach is to use a subwavelength unit cell approach [23], [59], [61]. The unit cell is a dielectric structure with an air void inside, whereby varying the size of air voids changes the effective permittivity of the unit cell.

One of the most widely used types of GRIN lenses is the Luneburg lens. A Luneburg lens is a spherical lens with a radial permittivity distribution from 2 at the centre of the lens to 1 at the outer surface [62]. This design enables a pencil beam radiation pattern. It provides wide-angle beam steering without a scan loss by placing several feeds along the surface of the lens. For 1D beam steering, a cylindrical cut of a spherical Luneburg lens can be used. The cylindrical Luneburg lens forms a fan-type radiation pattern.

A cylindrical lens consisting of 5 layers with different percentage of plastic infill was presented in [61]. The layers were separated at the transition between the different infill densities by a solid plastic wall which was observed to affect the lens performance. The actual thickness of the walls depends on FDM printer resolution. The percentage of plastic infill for each layer should be adjusted at the design stage according to the expected wall thickness. This approach is suitable for microwave applications when the thickness of the wall is much less than the wavelength.

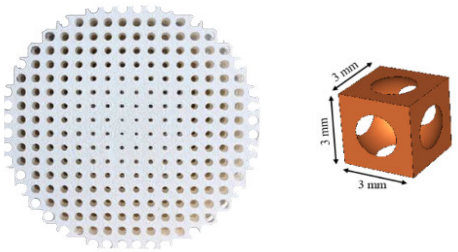

FIGURE 9. FDM-printed Ku-band Luneburg lens (a) and unit cell geometry (b) adapted from [63].

For example, [63] describes the design of a cylindrical Ku-band Luneburg GRIN lens using the PREPERM$^{\delta}$ low-loss material (Fig. 9). A dielectric cube with a spherical air void was used as the unit cell. By the use of a rectangular waveguide feed, the lens antenna was shown to have a gain of 23 dBi with side-lobes level of -12.5 dB at 15 GHz. This design was being considered for terrestrial satellite communications systems.

In [64], a unit cell approach for a Luneburg lens design was also used. A Peano-type space-filling curve was considered as a unit cell (Fig. 10). Such design enables the variation of air volume in the lens profile using a continuous curve. Hence, a quasi-continuous gradient of refractive index can be obtained. In this design, the surface of the lens was flattened. The flat surface makes it easier to integrate antenna feeds. The quasi-conformal transformation optics (QCTO) method was used to transform the spherical surface of the lens into a flat surface by recalculating the local distribution of the refractive index. FDM was used as the fabrication process with polycarbonate as the printing material. The material was characterized in the frequency range of 8-40 GHz. The dielectric constant $\varepsilon_r = 2.68$ and the loss tangent $\tan\delta = 0.0005$ were measured. An open-ended waveguide feed was used as a feed source. According to measurements with the source located in the central position, the realized gain of the lens antenna varied from 16.0 dBi at 26 GHz to 19 dBi at 40 GHz. The resulting design achieved a scanning angle from $-55°$ to $+55°$ in the Ka-band (26-40 GHz).

In [65], the application of an approach based on the combination of using geometric optics (GO) and the particle swarm optimization (PSO) method for inhomogeneous dielectric

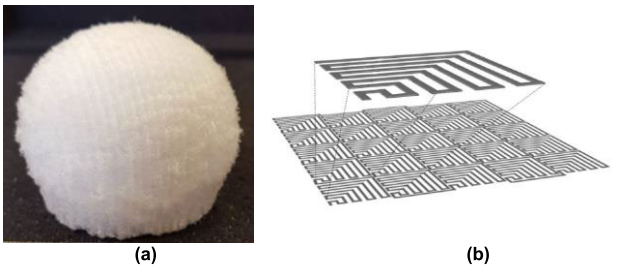

FIGURE 10. FDM printed modified Luneburg lens with space filling curves (a) and view of Peano-type space-filling curve (b) adapted from [64].

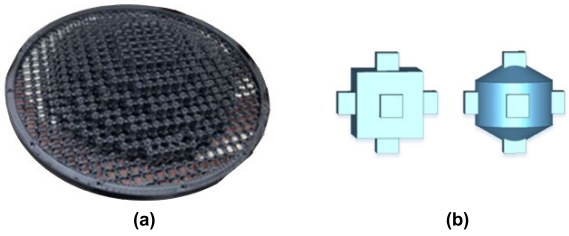

FIGURE 11. FDM-printed pixelized shaped inhomogeneous lens (a) and the cubic-based unit cell (left) design that cannot be printed in FDM and cylindrical unit cell with conical base (right) design (b) adapted from [65].

lens antennas was studied. The structure was firstly synthesized by using the GO method. After that, it was optimized by using the numerical PSO method (Fig. 11). This method is widely used for optimizing complex nonlinear functions, and parametric structural optimization. The positive aspects to this approach are that the method does not require a pre-defined gradient of the function, and there is low algorithmic complexity. Thus, the lens geometry and the permittivity function were described by using polynomials. The optimized lens design obtained using the GO/PSO methods was implemented by using cylindrical unit cells with a conical base, which allowed unit cells to be printed without protrusions and supporting structures. The high-temperature thermoplastic Ultem 9085 with low loss and low gas emission, suitable for space applications, was chosen as the material for FDM printing. The measured parameters at a frequency of 13.9 GHz for this material were $\varepsilon_r = 2.686$ and $\tan\delta = 0.012$. The measured directivity for the design was 20.58 dB at 13.4 GHz. The designs were also printed using MultiJet printing (MJP), however for the tough application of next-generation space weather radars, the FDM printing process and Ultem material are more suitable.

The Gutman lens is a generalized type of Lunenburg lens with a focal source located inside the lens. One drawback of this lens is the location of the feed inside the lens which limits the lens fabrication. A solution is to truncate the lens along the focal point. In this case, the feed antennas can be placed on the obtained surface. In [66], a Gutman lens designed for operation in the Ku-band was presented. The design of the lens was based on a cubic unit cell with a cubic air cavity. By varying the size of the internal cavity or/and plastic infill, a target dielectric constant can be achieved. The measured

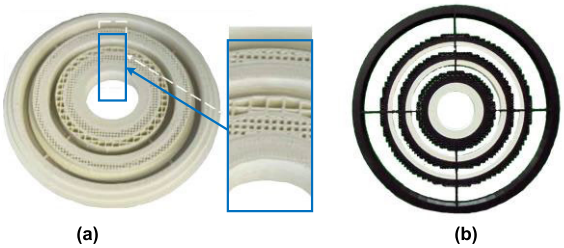

FIGURE 12. Hybrid Fresnel lens, with zoomed-in view of perforated zones that utilize the rectangular grid patterns (a) adapted from [70] and double material Fresnel lens (b) adapted from [71].

realized gain was 20 dBi with a 3 dB scan loss within ±45° scanning angle. This type of lens can find applications in next-generation satellites and 5G communication systems and radar technologies.

In [67] and [68], using FDM/FFF processes is considered from the point of view of reducing production costs and supporting more environmentally friendly technological processes. A six-layer planar GRIN lens fed by an X-band conical horn antenna was proposed. The measured gain was from 16 to 24 dBi over the frequency range from 12 to 18 GHz. The authors investigated the applicability of high dielectric plastic for printing planar Fresnel zone plate lenses. The commercially available PREPERM$^{\delta}$ thermoplastic with a dielectric constant of 4.4 was used. The PREPERM$^{\delta}$ filaments are designed for RF applications and the company provides the dielectric permittivity and loss tangent for solid filaments measured at 2.4, 22, and 60 GHz [69].

In [70] the design of a Fresnel zone lens (FZL) was considered. FZL has a thin profile and a short focal length antenna. It has a planar structure in comparison with a homogeneous dielectric lens (Fig. 12-a). In general, FZL consists of a series of concentric rings, known as odd and even Fresnel zones, respectively. In the presented design two different approaches to FZL implementation were combined. The first approach used a series of concentric grooves, but this approach suffered from the shadow blockage effect associated with designs with $F/D < 0.5$, where F is focal distance and D is the diameter of the lens. The second approach was based on perforated media with effective permittivity. In the hybrid design, the perforated FZL zones that had a size greater than the size of the unit cell were replaced by the grooved zones. The inner part of the lens was fabricated using the perforated structure. It minimized the shadow blockage and improved the gain and bandwidth of the lens compared with a grooved Fresnel Lens. The lens diameter was approximately ∼100 mm, and the feed was located at a focal length of 30 mm, which resulted in an F/D ratio of ∼ 0.3. As a feed, a WR28 open-ended waveguide (OEWG) was used. The lens was designed to operate at 33 GHz and the lens was made using PREPERM$^{\delta}$ TP20279 filament with $\varepsilon_r = 3$ and $\tan\delta = 0.0046$. The hybrid FZL was compared with the grooved Fresnel lens (GFL). The FZL and GFL have the same directivity below 33 GHz. Diffraction due to shadowing was negligible at the

lower frequency region, but at frequencies above 33 GHz the hybrid FZL demonstrated better performance. The operating bandwidth of the hybrid lens was ∼25%, and the realized gain ranged from 13.2 dBi to 25.6 dBi. In the frequency range of 26 - 40 GHz, the overall efficiency was from ∼74% to 95%, and the aperture efficiency was up to 31.1% at the centre frequency. The hybrid approach to the lens design enabled by additive manufacturing improved the directivity, overall efficiency, aperture efficiency, and bandwidth of the lens antenna.

A low-profile Fresnel lens antenna, which can be integrated into compact microwave wireless systems, was shown in [71]. FDM and SLA lens fabrication methods were compared. Four different materials were studied and their properties were characterised in advance. According to measured results the materials recorded the following parameters: for FDM printing PREMIX TP20280 $\varepsilon_r = 4.79$ and $\tan\delta = 0.0039$, STRATASYS ABS $\varepsilon_r = 2.61$ and $\tan\delta = 0.0036$, and for SLA printing SOMOS NanoTool $\varepsilon_r = 3.356$ and $\tan\delta = 0.015$, SOMOS 18120 with $\varepsilon_r = 3.16$ and $\tan\delta = 0.033$. Using the FDM process for lens implementation ensured a lower loss level in comparison with SLA. In contrast with [70], where the percentage of plastic infill was varied, in this design, two different materials were used for the single design (Fig. 12-b). The PREMIX thermoplastic was used to print the high dielectric parts of the lens, and the other parts were printed with the second material. At 22 GHz, the measured gain of the SLA lens was 27.3 dBi, and the FDM lens was 27.8 dBi. These results correspond to an efficiency of 30-35%. Beam steering was achieved in the range of ±25°. It was noted that printing with material with higher dielectric permittivity and bigger air gaps for implementing the same value of effective dielectric constant leads to increasing efficiency. It can be explained by decreasing of loss tangent of the material with air voids.

The design of a transformed hyperbolic flat lens operating in the 30 GHz band was presented in [72]. The lens was printed using ABS thermoplastic PREPERM ABS 1200 with a dielectric constant of 12 and $\tan\delta = 0.004$. The hyperbolic lens was compressed using transformation optics (Fig. 13). The given dielectric constant values were provided by changing the percentage of plastic infill of each section of the transformed lens, and an open WR-28 standard waveguide was chosen as the feed source. The directional properties of 3D printed transformed hyperbolic lens were comparable to the traditional hyperbolic lens. The full-wave EM simulations of the lens model with homogeneous layers were compared to simulated results of the model obtained from .gcode. The comparison of the simulated results showed a good agreement. Hence, recalculation of the effective parameters of the layers using a slicer was accurate. A graded refractive index lens antenna designed to emit 45° beamwidth in eight different sectors was presented in [73]. The lens can operate in two regimes: equal-phase and anti-phase excitation. Consisting of eight parts printed using FDM technology, this antenna provided 360° azimuth coverage with eight beams (Fig. 14).

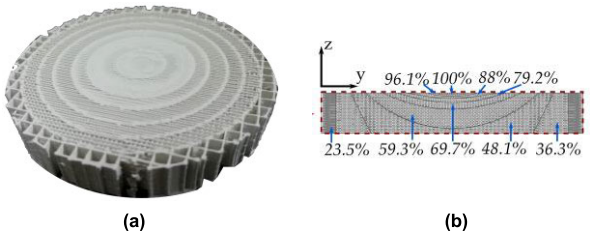

FIGURE 13. Transformed hyperbolic flat lens (a) and corresponding infill percentages for each permittivity value (b) adapted from [72].

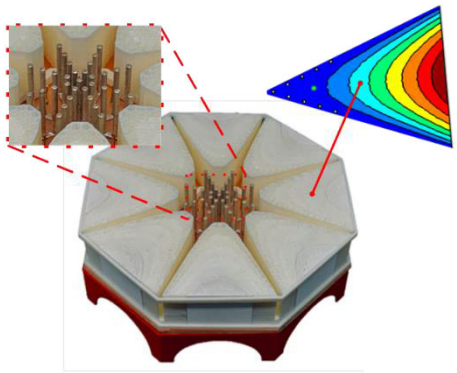

FIGURE 14. 3D printed lens prototype with embedded feeding structure positioned on a metallic ground plane (b) adapted from [73].

The realized gain of the single sector was 8.5 dBi, and in the case of multibeam operation, the maximum gain reached 5.9 dBi. Two different materials were used for printing: standard white ABS plastic from Verbatim and ABS-400 filament from PREPERM©. Both were characterized using a Keysight 85072A split-cylinder resonator operating at 10 GHz. Standard ABS from Verbatim had a dielectric constant of 2.69 and PREPERM ABS-400 had a dielectric constant of 3.99 with measured $\tan\delta = 0.002$ and 0.0015, respectively. During the two stages of printing, the inner and outer parts of the lens were made from these materials respectively. The feed source was a switched monopole array consisting of metal ports 13 mm long with reflectors, also printed on a 3D printer and coated with silver-plated copper.

FDM printing technology is one of the most accessible and popular on the market. That is why it is so popular for lens prototyping. The different types of the lenses fabricated using FDM is shown Table 1. Due to its relatively low accuracy and resolution, FDM fabricated lenses tend to find applications in the microwave range. Also, high surface roughness can be a limitation when a second step such as metal plating is required to realise the antenna design. These drawbacks can be overcome by using the SLA process.

B. GRIN LENSES BASED ON SLA PRINTING

The SLA process is based on the selective curing of polymer resins using ultraviolet rays. It enables the production of complex designs with high accuracy. It also produces parts with a low surface roughness and high uniformity. The wide range of materials for SLA printing opens up new opportunities

TABLE 1. FDM printed GRIN lenses.

Lens Type	Implementation	Radius of the lens	Operational frequency, GHz	Operational frequency band, GHz	Gain, dBi	Aperture Efficiency	Beam steering capability	Field of view	Ref.
Luneburg lens	Cubic unit cell with spherical air void	~80 mm	15	12-18	22.2	n/a	1D	n/a	[63] (2019)
Luneburg lens	Peano-type curve as unit cell	30 mm	30	26 - 40	16 - 19	n/a	2D	±55°	[64] (2019)
Inhomogeneous shaped lens with Luneburg-like permittivity profile	Cylindrical unit cell with conical base	60 mm	13.4	n/a	20.58	n/a	n/a	n/a	[65] (2018)
Fresnel lens	Recalculation the permittivity into a % of plastic infill + homogenous dielectric walls	48.8 mm	33	~25%	13.2 - 25.6	31.1%	n/a	n/a-	[70] (2022)
Fresnel lens	Recalculation the permittivity into a % of plastic infill + homogenous dielectric walls	90 mm	20	18 - 26.5	27 - 33	30-35%	2D	±25°	[71] (2019)
Hyperbolic flat lens	Recalculation the permittivity into a % of plastic infill	38 mm	30	30 GHz band	~21	n/a	n/a	n/a	[72] (2020)
GRIN lens	Recalculation the required permittivity into a % of plastic infill	The size is 172 x 172 mm and an aperture width of 70 mm for each segment	5.8	5.8 – 6.0 GHz	8.5 single beam, 5.9 multi-beam operation	n/a	1D	8 beams with 45° beamwidth covering 360°	[73] (2020)

for antenna design. The new materials for SLA printing are constantly under development to target decreasing losses as well as improving the mechanical properties. It must be noted that as-built SLA parts have lower mechanical properties compared to FDM parts and therefore antenna designers must consider the various trade-offs when selecting a process.

An SLA-printed broadband Luneburg lens was presented in [74] where the required gradient refractive index was realised by varying the radius of the dielectric cylindrical posts. The dielectric posts were built up between two plates, which were subsequently metalized by sputtering (Fig. 15), and a horn antenna was used as the feed source By using two metalized parallel plates, it was possible to excite two orthogonal modes and realize circular polarization. The results showed that the lens antenna provided a frequency bandwidth of 43% (21- 32.5 GHz) with a reflection coefficient of less than -10 dB and the axial ratios less than 3 dB, and a gain of approximately 12 dBi. Through the placement of multiple feed sources, this lens could achieve multibeam operation. This work is an example of the combination of SLA technology and metal plating. The surface roughness was Ra $=$ 2.91 microns before metallization for SLA and Ra $=$ 5.89 microns for FDM, which was used for printing the horn antenna. Metal plating led to a further decrease in surface roughness. This work illustrates the possibility of combining various inexpensive processes for the quick and accurate production of lens antennas.

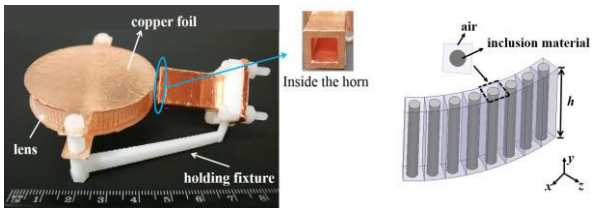

FIGURE 15. Assembled fabricated Luneburg lens with holding fixture (inset: inner surface of the feeding horn) (a) and unit cells realized as dielectric posts (b) [74].

A flat Luneburg lens antenna operating at 60 GHz was considered in [75]. A cube with a cubic air void was used as the unit cell and the size of the unit cell side was 1 mm. The diameter of the entire lens was 30 mm (Fig. 16) and it was printed using a polymer resin with measured parameters $\varepsilon_r = 2.9$ and $\tan\delta = 0.015$. The WR-15 rectangular waveguide was used as a feed source. At 60 GHz, the gain was approximately 15.3 dB. The main lobe beamwidth in the E-plane was 11.5 degrees with the side lobes level - 12 dB. The measured gain of the lens antenna varied from 14.1 dB at 57 GHz to 16 dB at 64 GHz.

The advantage of the Fresnel-zone plate lens is a planar structure, but for GRIN lenses it is also possible to convert some volumetric or spherical designs to flat designs by using transformation optics (Fig. 17) [76]. A flat lens antenna

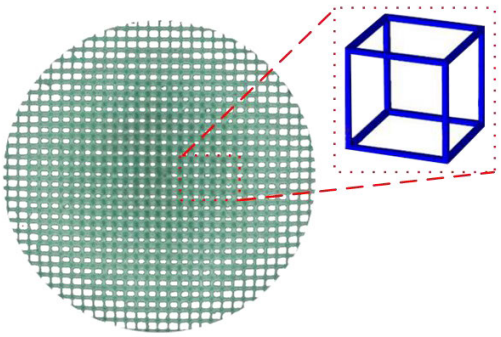

FIGURE 16. Flat Luneburg lens antenna with the unit cell design adapted from [75].

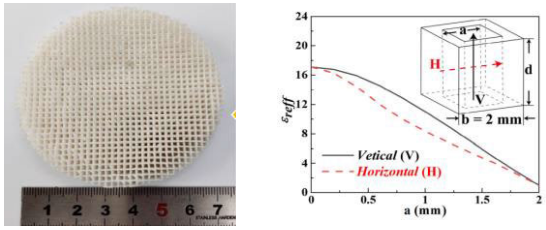

(a) (b)

FIGURE 17. Flattened Luneburg lens: prototype (a) and dependence of effective dielectric permittivity of unit cell from air void size (b) [76].

converted from a Luneburg lens with a horn feed operating in the Ku band (12-18 GHz) was considered. Using the method of transformation optics enabled the thickness of the lenses to be reduced to 78%. The diameter and thickness of the lens were 70.9 and 7.9 mm respectively. The results showed that the measured realized gain increased from 10 dBi to 19.1 dBi when compared to the horn antenna. In addition, the ability of a flat Luneburg lens to perform passive beam scanning with limited scan losses was demonstrated. In order to further reduce losses in the material, non-commercial materials were developed based on a ceramic suspension $MgTiO_3$ that had $\varepsilon_r = 17.1$ and $\tan\delta = 0.0002$. The results demonstrated that by using SLS low loss performance was achievable.

Until recently, the application of 3D printing for designs that operate at THz frequencies was difficult due to the limited accuracy and properties of materials. However, now more and more THz designs can be found. For example, [77] presented a modified Fresnel lens with circular polarization operating at 300 GHz (Fig. 18). The design consisted of discrete dielectric subwavelength posts for odd Fresnel zones. A linearly polarized open-ended waveguide was chosen as the feed source. In order to improve printing resolution and compliance with the design geometry, a layer thickness of 25 microns was used. The measured results shown that the axial ratio of the fabricated antenna prototype was less than 3dB for the bandwidth from 265 to 320 GHz, and the maximum gain was 27.4 dBi. It was only 0.9 dB less than a conventional Fresnel zone plane antenna (FZPA).

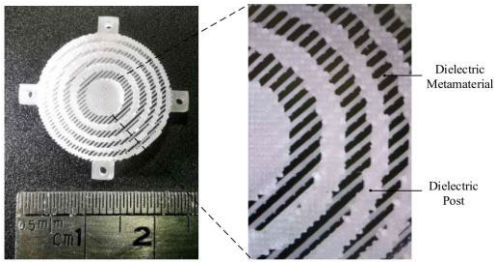

FIGURE 18. Modified Fresnel lens antenna for THz application [77] ©2019 IEEE.

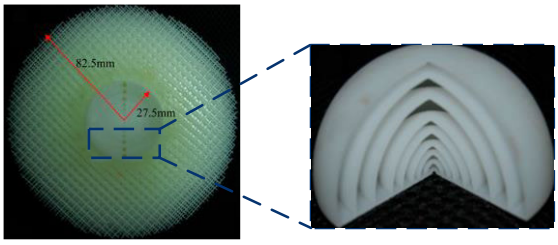

FIGURE 19. SLA-printed Eaton lens with compound liquid media adapted from [78].

An Eaton lens is a type of gradient index lens with spherical or transversely cylindrical symmetry. Due to a special distribution of the refractive index, the Eaton lens changes the direction of propagation of the electromagnetic wave, essentially turning it. In [78], an approach to implementing an Eaton lens by combining non-resonant GRIN woodpile photonic crystals structure with a compound liquid medium was proposed (Fig. 19). Such a design was considered to provide a large range of refractive indices values with broadband performance. The lens consisted of two parts printed using SLA. The outer part was a sphere combined from unit cells filled with air, and the second part was made as a sphere with liquid inside. The outer diameter of the first part was 82.5 mm, and the outer diameter of the second part was 27.5 mm. According to experimental data, the effect of omnidirectional wave bending in a wide operational frequency band (12-18 GHz) was feasible.

Some GRIN lenses have a spherical shape, and these designs in the case of multibeam operation are faced with the problem of locating the feeds along spherical or cylindrical surfaces. Using a transformational optics approach [20], [24], [64], [80], [81] helps to convert the spherical focal surface into a flat surface. An all-dielectric planar Mikaelian lens antenna was considered in [79]. It was designed using ray tracing and provided 1-D beam-steering (Fig. 20). Five rectangular microstrip patch antennas operating at 10 GHz were used as feeds. The size of the lens was 168.8 mm x 147.8 mm with a thickness of 25mm. A cubic unit cell with cylindrical voids was used. The material used for printing was resin C-UV 9400E with $\varepsilon_r \approx 2.8$, and $\tan\delta \approx 0.02$. The beam scanning was achieved within a field of view $\pm 20°$ with a realized gain of $\sim$13.2 dBi and a side lobes level less than -11.5 dB.

TABLE 2. SLA/DLP printed GRIN lenses.

Lens Type	Implementation	Radius of the lens	Operational frequency, GHz	Operational frequency band, GHz	Gain, dBi	Aperture Efficiency	Beam steering capability	Field of view	Ref.
Luneburg lens	Cylindrical posts	23.8 mm	26.75	21–32.5	~12	26 - 57%	1D	n/a	[74] (2020)
Luneburg lens	Cubic unit cell with cubic air void	15 mm	60	57 - 64	14.1 - 16	n/a	1D	n/a	[75] (2019)
Fresnel lens	Dielectric posts	9.51 mm	300	265 - 320	27.4 dBic	15.4%	n/a	n/a	[77] (2019)
Eaton lens	Compound liquid medium with dielectric unit cell	82.5 mm	15	12-18	n/a	n/a	n/a	90°	[78] (2014)
Mikaelian lens	Cubic unit cell with cylindrical voids	168.8 x 25 mm	10	~4% (lim. patch antenna)	13.2	n/a	1D	±20°	[79] (2021)

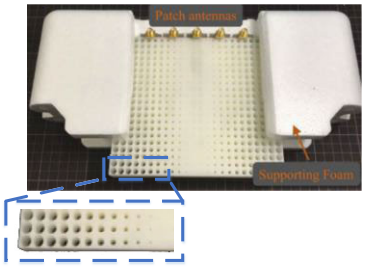

FIGURE 20. Fabricated Mikaelian lens antenna prototype adapted from [79].

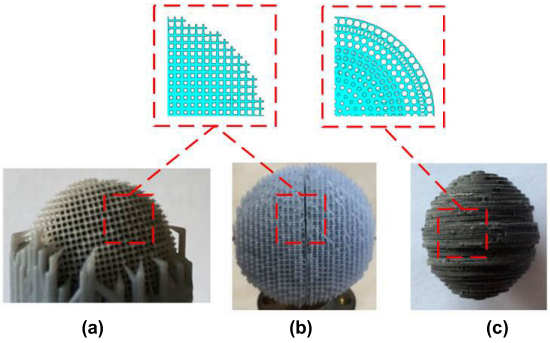

FIGURE 21. The fabricated Luneburg lens, (a) 3D printing– Formlabs, (b) 3D printing – Prusa, (c) CNC– substrate drilling adapted from [82].

A comparison of subtractive and additive manufacturing for the design of the W-band Luneburg lens was presented in [82]. In the case of the subtractive manufacturing, the lens was fabricated as a set of thin perforated layers of a Rogers RT5880 with $\varepsilon_r = 2.24$, which were interconnected by an adhesive material (Fig. 21-c). The diameter of the lens was 24.5 mm. The measured gain at 80 GHz was 24.6 dBi. It was concluded that the disadvantages of the subtractive method were increased manufacturing time and the potential displacement of individual layers, which may lead to degradation of the characteristics of the lens. Some anisotropic properties of the substrate may affect the directional characteristics of the antenna. The spherical lens of the same size was produced by using additive manufacturing (Fig. 21-a, b). A cross-type unit cell was used, and UV-curable resins V4 FLGPGR04 and Grey Touch were used as the printing material. The 3D-printed lens antenna had a realized gain of 18.18 dBi which was significantly lower than the simulated model. The difference was caused by the imperfection of the printed model and its assembly. Also, the dielectric constant and losses of the adhesive locally violated the effective permittivity. The results further demonstrated the subtle difference that minor local changes to the material properties can have on the overall system performance.

A broadband GRIN lens with a modified refractive index profile based on a periodic structure with a radial gradient was examined in [83]. The difference from other implementations was the discretisation of the lens profile into 33 layers and the variation of the refractive index from 1.26 at the outer surface to 1.6 at the centre (Fig. 22). Changing the permittivity distribution made it possible to improve the sub-diffraction focusing of the lens. Gradient periodic structures were represented as inverted Y-shaped unit cells. Photocured resin Vero White Plus 835 with a dielectric constant of 2.8 was used. This lens was considered for sub-diffraction imaging and a highly efficient achromatic lens with sub-diffraction focusing was obtained. The focusing efficiency reached more than 74% in the range from 8 to 16 GHz. The measured results showed a good agreement with the simulated model due to the proper choice of material parameters for simulations and unit cell design which correspond to printer resolution.

SLA printing technology allows the production of different types of the GRIN lenses and supports extremely high accuracy and resolution. It can be used for lens implementation from microwave to sub-THz applications (Table 2). This printing method is characterized by low surface roughness, which can be useful for structures that need to be coated by metal.

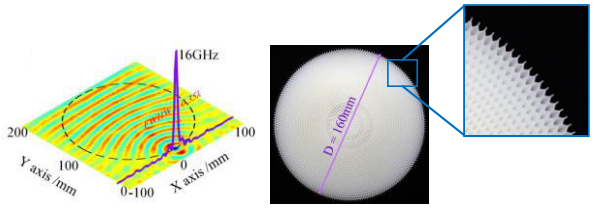

FIGURE 22. The electric field distribution at 16GHz (a) and the fabricated modified Luneburg lens (b) [83].

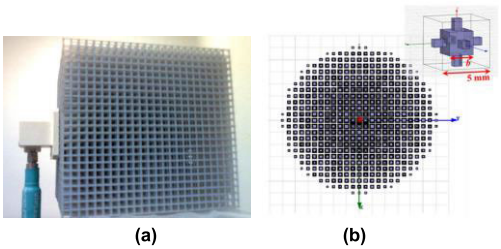

FIGURE 23. JM-printed Luneburg lens fed by a waveguide (a) and lens model with cubic inset (b) [86] ©.

C. JETTING MODELING FOR GRIN LENS DESIGN

This technology is in many ways similar to conventional inkjet printing. The technology has the potential to use multimaterials such as conductive inks, liquid photopolymers or waxes, and therefore offers considerable design freedom for complex RF structures. There are a number of examples of fully printed antenna design using this technology [84], [85]. With the development of JM it could be possible to print conductive and non-conductive material in one production cycle which is a significant enabler, ahead of competing technologies.

Using different dielectric materials simultaneously is possible due to the presence of several nozzles in the printhead. UV radiation is used to cure the material, similar to SLA technology. The advantage of this approach is the high resolution of printed parts due to the ability to print a layer with extremely small thickness. A large selection of materials and the parameters enable parts with complex geometries. However, at this time, the technology has not yet become widely used for lens antenna design. This can be attributed to the high capital equipment cost and market availability of JM printers compared to FDM or SLA printers.

The Luneburg lens is often fabricated using 3D printing, and earlier Luneburg lens designs using FDM [64] and SLA [75] printing were reviewed. In [86] the applicability of JM printing for a Luneburg lens was considered. The material which was used for printing has a loss tangent of 0.02. It is higher than in [64] and [75] which can lead to lower antenna efficiency. The implementation of the lens was based on the use of a cubic unit cell with a variable edge size from 0 mm to 5 mm (Fig. 23). Each cubic cell was connected to its neighbours using connecting rods with a diameter of 0.8 mm. The diameter of the lens was 120mm. The measured gain of the antenna in the X-band was from 17.3 to 20.3 dB. The half-power beamwidth was from 19° to 12.7°. The side lobes level was approximately −25 dB. This design can be used in radar reflectors to increase radar visibility.

A cylindrical Luneburg lens using JM was shown in [87]. The antenna consisted of a low-profile cylindrical Luneburg lens-based planar beamforming network, a folded double-layer guided-wave structure, and a leaky-wave antenna array (Fig. 24). All three parts were made using JM. The postprocessing metallization technology for parallel plate waveguide and a leaky-wave antenna array was also used. A radially

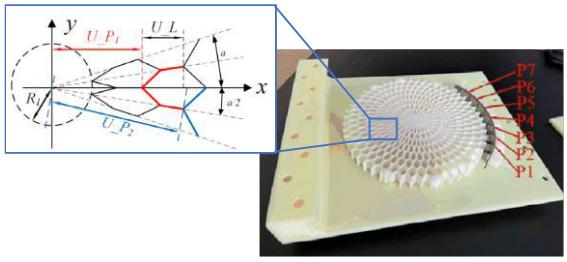

FIGURE 24. Cylindrical Luneburg lens: view of hexagonal-like unit cell and printed prototype adapted from [87].

located microstrip antenna array was used as a feed source. The printed cylindrical Luneburg lens used a hexagonal-like unit cell. The design of the Luneburg lens in conjunction with the leaky-wave antenna array helped to increase the efficiency of the antenna. This lens antenna allowed scanning in the range of ±29° and supported seven beams with a minimum crossover level of −2.5 dB. The gain was 19.8 dB at 10 GHz, and a scan loss was 2.7 dB. The dipole/slot antenna array for Ka-band was printed and electroplated [88].

In [89], a Luneburg lens for 5G millimetre-wave multiple-input multiple-output applications was presented (Fig. 25). The rod-type structures were employed as the unit cell. The substrate-integrated waveguide-fed magnetoelectric-dipole antenna with an endfire radiation pattern was used as a feed source. The lens was printed using VeroClear photopolymer with $\varepsilon_r = 2.9$ and $\tan\delta = 0.01$. Due to the choice of the feed sources, the antenna was broadband and provided operation in almost the entire Ka-band. The antenna formed nine beams that could cover an angular sector of ±61°. The realized gain at the central frequency is 21.2 dBi with a scanning loss of 2.6 dB. The estimated radiation efficiency of the manufactured prototype was approximately 75%.

In [90], a dielectric planar lens (Fig. 26-a,b) with a fixed beam and a beam scanning capability for the mm-wave application was considered. To adjust the dielectric constant, square dielectric posts of variable height were used. Additionally, periodic antireflection structures were implemented to reduce the impedance mismatch at the air-dielectric interface (Fig. 26-c). This approach to the lens design enabled improved directional properties of the antenna. The lens antenna operating at 60 GHz was fed by a WR-15 open-ended waveguide. According to the results of the near-field

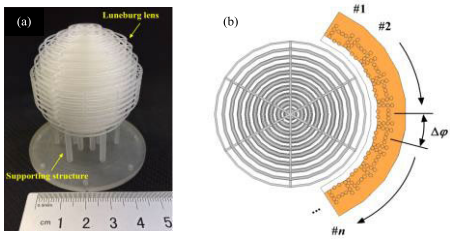

(a) (b)

FIGURE 25. Multi-beam Luneburg lens antenna with radial rod-type unit cells: prototype (a) and model (b) [89].

measurement, the gain was from 19.4 to 23.5 dBi within the operational frequency band. The frequency beam scanning was demonstrated for the proposed lens design.

The lens with a fixed beam and a frequency scanning beam for the THz range was also presented in [90]. The size of the lens for the THz application (220 – 325 GHz) was approximately 14 mm. The WR-3 open-ended waveguide was used as a feed source. The measured side lobe level was below −22 dB and −27 dB in the E- and H-planes, respectively. The measured gain was shifted down about 20 GHz and 2 dB less than the simulated one which could be explained due to the uncertainty of the dielectric properties of the material at THz frequencies.

For the design of lens antennas, various optimization algorithms can be applied. For example, in [91] two consecutive optimization processes based on the particle swarm optimization (PSO) method were used to design a mm-wave GRIN lens (Fig. 27). Firstly, the geometric optics approach was applied to the lens design, then the parameters of the lens (the dielectric constant and dimensions) were optimized. After that, the magnitude and phase distributions over all radiating elements were optimized by the PSO algorithm. A phased array antenna feed with aperture-coupled microstrip antenna elements was used as a feed antenna. At 28 GHz, the aperture size was 10λ. The design consisted of several parts embedded into each other and connected by adhesive. Two materials were used for the printing process with $\varepsilon_r = 3.7$, $\tan\delta = 0.005$ and $\varepsilon_r = 2.9$, $\tan\delta = 0.01$ at 28 GHz. The gain was from 21.4 to 24.5 dBi in the scanning sector ±58 degrees. The gain drop between simulated and measured results was explained by simplifications adopted in optimising power and phase distributions, as well as dielectric losses in the antenna array and lens.

The Eaton lens (Fig. 28-a), which rotates and collimates electromagnetic radiation, was presented in [92]. The model consisted of an inner solid sphere with a diameter of 112.3 mm and an outer spherical shell composed of cubic unit cells with a size of 5 mm (Fig. 28-b). A material with $\varepsilon_r = 2.7$, $\tan\delta = 0.02$ with thin polymer rods were used as support for the entire structure. A WR-90 open-ended waveguide was used as a feed source. The Eaton lens could deflect the beam with a bent angle of 37° in the X-band.

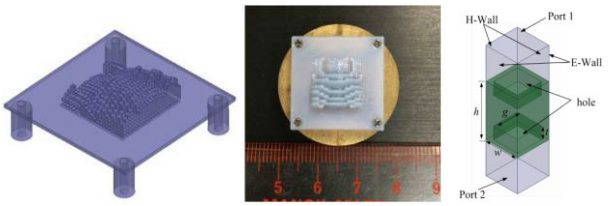

(a) (b) (c)

FIGURE 26. THz lens model (a), prototype (b) and view of antireflecting layer (c) [90].

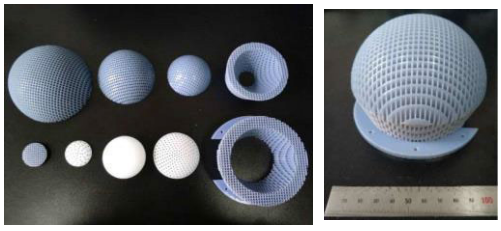

(a) (b)

FIGURE 27. Mm-wave GRIN lens: separate parts (a) and assembled prototype (b) [91].

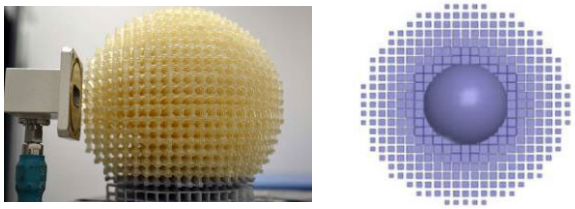

(a) (b)

FIGURE 28. Eaton lens: prototype (a) and model (b) [92].

The gain was 13 dB at 10 GHz. The use of GRIN structures is not limited to lens antennas in the traditional realization. In [93], the GRIN structure was integrated into the horn antenna (Fig. 29). A shortened horn antenna in combination with a flat GRIN inset was designed to increase directivity. This design enabled an increase in directivity up to 14.6 dB at 15 GHz, which was 6.2 dB higher compared with a horn antenna without it. The lens was used to collimate the radiation and reduce the phase errors of the horn antenna. The lens itself was a lattice block with a width of 6 mm and a length of 84 mm, consisting of unit cells of various sizes. The ceramic material zirconium dioxide (ZrO_2) was used for printing to ensure a wide range of dielectric properties and better mechanical stability.

An overview of JM printed GRIN lenses is shown in Table 3. Various frequency ranges from microwave to THz can be achieved using this technology.

D. SLS/SLM GRIN LENS IMPLEMENTATION

FDM and SLA technologies often suffer from poor mechanical properties. Designs that require higher robustness, where strength, ductility and robustness to atmospheric conditions are important, the SLS/SLM can be used. The advantage of

TABLE 3. JM printed GRIN lenses.

Lens Type	Implementation	Radius of the lens	Operational frequency, GHz	Operational frequency band, GHz	Gain, dBi	Aperture Efficiency	Beam steering capability	Field of view	Ref.
Luneburg lens	Cubic unit cell	60 mm	10	8-12	17.3 – 20.3	40 – 60%	2D	n/a	[86] (2014)
Luneburg lens	*N*-shaped gradual thickness unit cell	7.9×6.5 mm	10	n/a	17.1 - 19.8	8.0 - 14.9%	1D	±29°	[87] (2021)
Luneburg lens	3D dielectric rings	24 mm	33	26-40 GHz	18.6 - 21.2	35 – 49%	1D	±61°	[89] (2019)
THz dielectric planar lens	Dielectric posts	10.5×10.5 mm	275	225 - 325	15 - 27.5	n/a	1D	±33.3°	[90] (2016)
GRIN lens	Radically stratified hemispherical shells	~107 mm	28	27 - 29	max 28.2	max 67.5%	2D	±58°	[91] (2020)
Eaton lens	Cubic unit cell	60 mm	10	8-12	13	n/a	n/a	90° bend of the beam	[92] (2016)

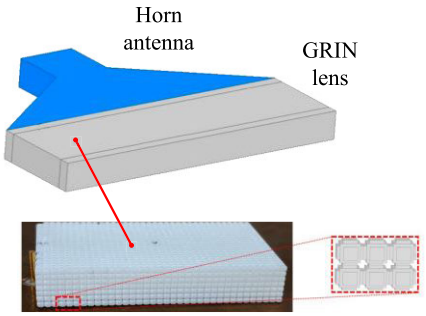

FIGURE 29. Inset to the horn antenna adapted from [93].

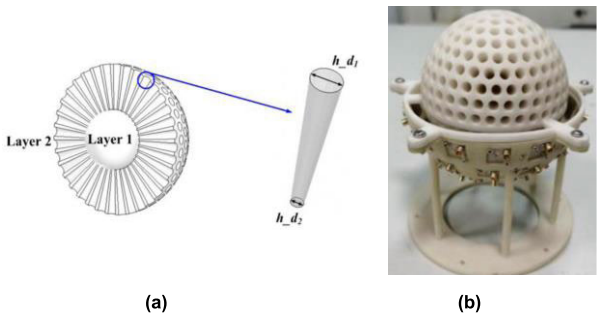

FIGURE 31. Two-layer spherical lens antenna: model (a) and printed prototype with conformal feed placement (b) [94] ©2021 IEEE.

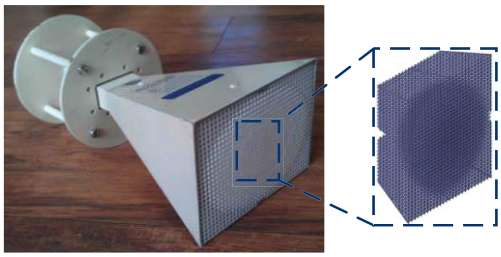

FIGURE 30. Half ellipsoid GRIN lens model and view of antireflecting layer adapted from [10].

SLS/SLM technologies is the high strength of the parts produced, and support structures are not required in SLS, since the powder itself acts as the support. Due to the usage of fine powder with a defined size, the final surface roughness of the SLS/SLM printed parts is good. Sometimes additional post-processing polishing is needed when conductive materials are printed. It is difficult to print large flat surfaces and small holes since internal stresses occur during sintering/melting. Hence, SLS/SLM parts are more susceptible to shrinkage and deformation than others. Additionally, these technologies are implemented in professional and expensive printers, and skilled operators are required, particular for SLM. Hence, the number of publications with SLM/SLS lens design is less than FDM and SLA.

In [10], a half ellipsoid Luneburg GRIN lenses placed inside a WRD350 and WRD750 horns antenna were printed and investigated (Fig. 30). Nylon PA2200 with $\varepsilon_r = 2.4$ was used as the material for SLS printing. The lenses were realized using a cubic unit cell with spatially varying air voids. According to measurements in the frequency range 3.5-8.2GHz and 7.5-18GHz, improvements in broadband performance, side lobe level suppression, and directional properties were achieved.

GRIN lenses are often used to improve scanning capability and widening of the field of view. A two-layer spherical lens antenna with a large coverage sector was presented in [94]. A U-shaped patch antenna with circular polarization was used as a feed source. An array of feeding antennas was provided with 2D beam scanning (Fig. 31). The lens itself was an internal solid sphere and an external one consisting of unit cells. The unit cell was in the form of radial conical holes with a gradient diameter. Some parameters of the two-layer spherical lens were jointly optimized to increase the antenna

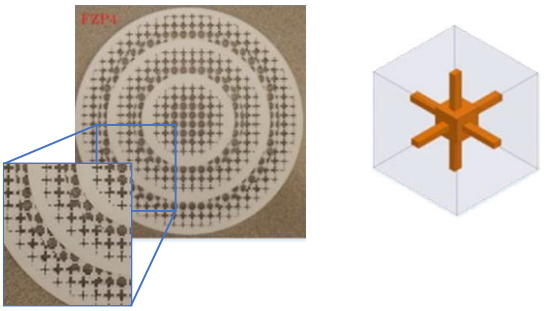

FIGURE 32. Fresnel-zone plate lens antennas for V-band (a) and unit cell view (b) adapted from [95].

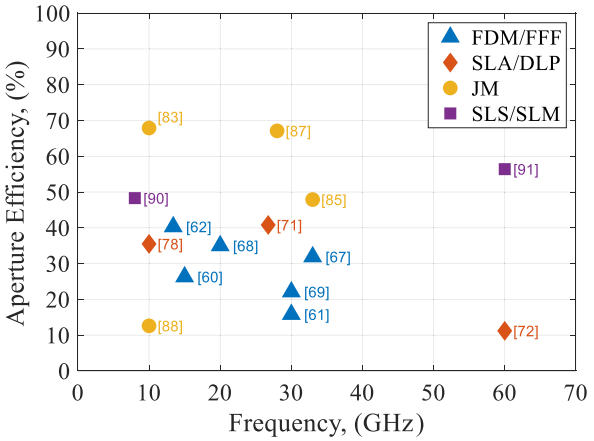

FIGURE 33. Aperture efficiency of the GRIN lenses.

gain. The lens was printed from PA3300 material with an $\varepsilon_r = 2.7$ and $\tan\delta \approx 0.005$ at 8 GHz. A supporting structure for the feeding antenna array was designed separately, which was printed from GF3400 material with $\varepsilon_r = 3.2$ and $\tan\delta \approx 0.01$. The measured gain varied in the range of 14.3–15.3 dBi for 7.7–8.2 GHz. The beams in the elevation plane can cover sector $\pm 90°$, so this makes it promising for application in satellite communication.

In [95], fully dielectric Fresnel-zone plate lens antennas for V-band operation were investigated. The proposed lenses were designed with half ($\lambda/2$) and quarter ($\lambda/4$) phase correction rings. The lens diameter was $30\lambda_0$ at 60 GHz. The article examined both FDM and SLS technologies. For SLS printing, nylon PA 2200 was used, which was a non-filled powder based on PA-12 with $\varepsilon_r = 3.6$ and $\tan\delta = 0.068$. Quarter-wave Fresnel-zone plate lens had three circular flat zones, the space in between was filled with a structure consisting of cubic unit cells (Fig. 32). The maximum measured gain was 38 dBi at 65 GHz, and the half-power beamwidth of the proposed quarter-wave FZPA was 1.8°. The side lobe level was −26 dB. A horn antenna was used as a feed source. This type of antenna was not only cheap, and fast to produce, but also provided a pencil beam-type radiation pattern.

SLS/SLM process can be very promising for lens antenna design (Table 4). Especially when more powders with RF parameters will become commercially available. Future developments can have considerable advantages by

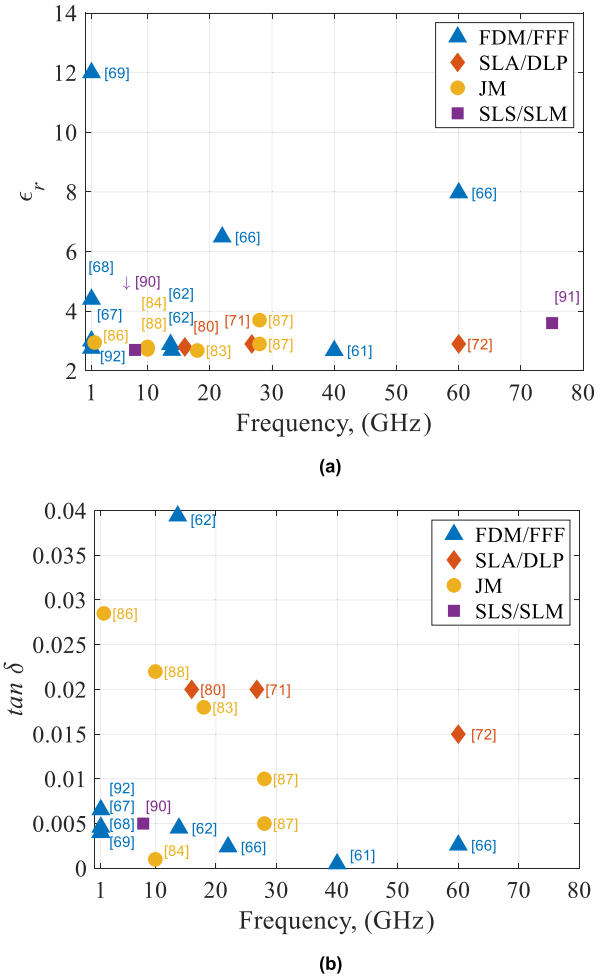

FIGURE 34. Dielectric constant (a) and loss tangent (b) for materials which were used for lens antenna designs.

combining metal and dielectric printing in the single manufacturing cycle.

E. COMPARISON OF THE GRIN LENS DESIGNS

Different types of lens antenna designs fabricated using four types of additive manufacturing processes were considered. Due to differences in types, sizes, and frequency ranges it is difficult to draw direct comparisons. In order to summarize the review, the aperture efficiency of some of the lenses was calculated based on data presented in the publications. The following equation was used:

$$e_a = \frac{G\lambda^2}{4\pi A_{phys}}, \tag{1}$$

where G is the gain, λ is the wavelength, A_{phys} is the size of the aperture.

For GRIN lenses, as for all-dielectric structures, aperture efficiency is mostly affected by the loss tangent of the dielectric material. In addition, it is important to consider the type of unit cell which will be used. The printing accuracy also plays a role as it can affect the aperture efficiency especially at higher frequencies. As shown in Fig. 33 FDM-printed GRIN lenses have relatively low aperture efficiency. Operational

TABLE 4. SLS/SLM-printed GRIN lenses.

Lens Type	Implementation	Radius of the lens	Operational frequency, GHz	Operational frequency band, GHz	Gain, dBi	Aperture Efficiency	Beam steering capability	Field of view	Ref.
GRIN lens	Conical unit cell	50 mm	8	7.7-8.2	14.3–15.3	38–49.6%	2D	±90°	[94] (2021)
Fresnel-Zone Plate Lens with λ/4 phase correction	Cube-shaped unit cell	75 mm	60	40-75	36-38	40-45%	n/a	n/a	[95] (2018)

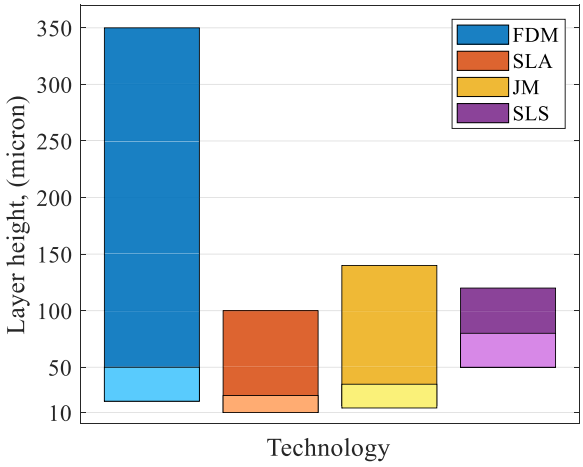

FIGURE 35. Resolution of 3D printing technologies (a light colour bars are for high-resolution commercially available printers).

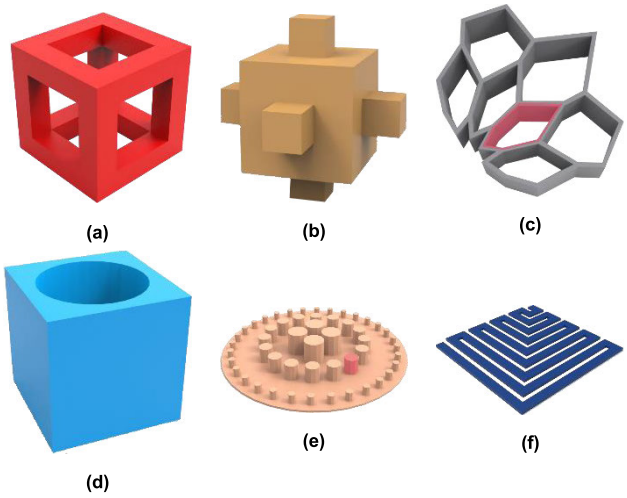

FIGURE 36. Unit cell designs: cube with cubic air void (a), solid dielectric cube (b), hexagonal (c), cube with cylindrical air void (d), solid cylinder (e) and Peano-curve (f).

frequency of FDM-printed GRIN lens is limited by low printing accuracy and resolution.

F. GRIN LENS DESIGN RECOMMENDATIONS

Considering the range of additive manufacturing processes and the complexity in GRIN antenna design, it is clear that there is an iterative development cycle that needs to take place over time. For example, RF antenna and lens designers need to get accustomed to the capabilities of 3D printing processes and their limitations, and this will in turn drive developments in 3D printing, e.g. more appropriate RF characterised material sets, multimaterials, higher accuracy etc.

This overview can help make the first steps towards 3D-printing of GRIN lens antennas. Based on requirements for directive properties or application, one type of lens can be chosen. For example, Luneburg, Gutman, Fresnel, etc. The lens choice defines the permittivity profile which is characterized by the maximum and minimum values of the permittivity [96]. The maximum value will dictate the material choice for printing. For RF, microwave, and even mm-wave applications, some materials with pre-defined EM parameters for FDM printing are available on the market. For SLA printing, most resins are not specified for antenna applications and must be additionally characterised. For SLS/SLM technologies, the focus is on the mechanical properties of the materials and not on the EM parameters, which means that EM characterization is also required. Nevertheless, there is currently a relatively wide selection of materials which can be chosen across all 3D printing technologies, and it can be foreseen that more EM characterised materials will enter the market place in the future.

Material parameters are summarized and shown in Fig. 35. It was shown that on average, most materials have a dielectric constant from 2 to 4. Adding ceramic particles with a high dielectric constant to the host material increases these values up to 20. Fig. 35-b presents the loss tangent ($\tan\delta$) versus frequency for different types of 3D printing processes. The loss tangent of a dielectric material quantifies dissipation of the electromagnetic energy due to different physical processes.

The next step with choosing the appropriate technology for manufacturing is the operational frequency band of the GRIN lens which can immediately result in a refined set of available 3D printing processes Hence, the size of the unit cell should be subwavelength and fit the printing accuracy and resolution.

The comparison of the resolution for different printers which are available on the market is shown in Fig. 35. FDM technology is characterized by the wide range of 3D printers for in-house applications with an average resolution of 50-350 microns [97]. The high-resolution FDM printers can print a layer with a height of up to 20 microns [98]. The 10 microns can be achieved by SLA printing [99], but the most common values are 25 - 100 microns [100]. In general JM printers ensure similar parameters [101], and high-performance JM printers can provide a resolution of

up to 15 microns [102]. For SLS process resolution can be about 50 microns [103].

Examples of unit cell designs are shown in Fig. 36. The most popular ones are cube (Fig. 36-a,b,d) or cylinder (Fig. 36-e). It is important to note that the choice of the unit cell depends on the polarization of the feed antenna. The effective dielectric constant of the unit cell with a central symmetry (Fig. 36-a,b) is invariant to the polarization of the feed antenna. For the rest of the unit cells, it is necessary to consider the polarization of the feed antenna during EM simulation and extraction of the effective parameters.

Based on the obtained dependence of the effective dielectric constant on the paraments of the unit cell, the full EM model of the lens can be obtained and simulated.

IV. CONCLUSION

3D printing presents new opportunities for fast and cheap lens antenna fabrication, especially GRIN lens antennas. The applicability of additive manufacturing to the design of antennas and components for wireless communication systems has become a driving force for companies that produce 3D printing equipment and consumables. They have put efforts to develop special materials which will be characterized for electromagnetic applications. The advancements of 3D printing equipment have led to improved resolution and accuracy, which enables lens antenna design in the sub-THz and THz operational bands.

Depending on the application, operational frequency band, the necessity of metal postprocessing, or any other type of postprocessing, different types of 3D printing can be applied to lens antenna design. For fast and cheap prototyping with relatively low accuracy, FDM printing can be chosen. FDM printers and consumables are relatively cheap. The process is user-friendly and does not require any special conditions or user abilities. FDM can be used for non-conductive and conductive materials. The conductive filaments suffer from low conductivity right now, but this segment of the market is really under development and significant improvement in conductivity is expected in the future. In addition, suppliers are reporting the EM properties of the materials now as standard similar to how mechanical properties are reported in the product specifications. The poor surface roughness of the FDM printed component can be a problem if metal plating is required as this leads to increasing losses in the structure. The other drawback is printing resolution which is limited by the size of the nozzles. For GRIN lens antenna design, this means that it is hard to realize the low values of effective dielectric permittivity close to one and hard to implement extremely fine details of the model.

The two main FDM disadvantages can be overcome by SLA, which is characterized by high resolution enabling the capture of fine details and extremely low surface roughness. For GRIN lens design, the challenge lies in the printing of small air voids inside the fully dielectric unit cells. The voids can suffer from inaccurate shape or size due to the surface tension forces of the liquid resin. This can be partially improved by choosing the proper unit cell geometry, model orientation and placement on the printing table. Due to the low surface roughness, SLA models are an ideal candidate for metal plating. In order to improve the mechanical properties of SLA parts, UV-curing is required post printing. However, parts with fine details can still be brittle/fragile which limits their application in use cases where robustness is important.

In contrast to the aforementioned processes, both SLM and SLS manufacturing are relatively expensive and require skilled operators, however, they produce parts with good mechanical properties. Also, complex metal parts can be fabricated which cannot be realised using traditional methods such as machining. Due to the high surface roughness, postprocessing polishing is obligatory for high frequency applications. This makes the process more complicated and expensive.

In the future, jet printing techniques can be used for conductive and non-conductive materials in the same manufacturing cycle. Nowadays it is supported by two different jet printing processes. The advantage of JM is the high resolution which can be obtained. The drawback is that conductive inks with high conductivity can be very costly.

For further development of 3D printed GRIN lens design, it is important to have a variety of the materials with characterized EM properties over wide frequency range. For increasing the antenna efficiency materials with low loss tangent should be available on the market.

In the future for extending GRIN lens application, for example outdoor, 3D printed parts have to provide strength, ductility and robustness to atmospheric conditions.

The choice of printing technology can be defined by antenna application and cost requirements. Then, based on the GRIN lens design, including the type of the unit cell, requirements for material parameters, resolution and accuracy, a suitable process can be chosen.

REFERENCES

[1] B. T. Malik, V. Doychinov, S. A. R. Zaidi, I. D. Robertson, and N. Somjit, "Antenna gain enhancement by using low-infill 3D-printed dielectric lens antennas," *IEEE Access*, vol. 7, pp. 102467–102476, 2019, doi: 10.1109/ACCESS.2019.2931772.

[2] J. Ala-Laurinaho, J. Aurinsalo, A. Karttunen, M. Kaunisto, A. Lamminen, J. Nurmiharju, A. V. Räisänen, J. Säily, and P. Wainio, "2-D beam-steerable integrated lens antenna system for 5G E-band access and backhaul," *IEEE Trans. Microw. Theory Techn.*, vol. 64, no. 7, pp. 2244–2255, Jul. 2016, doi: 10.1109/TMTT.2016.2574317.

[3] A. Bisognin, N. Nachabe, C. Luxey, F. Gianesello, D. Gloria, J. R. Costa, C. A. Fernandes, Y. Alvarez, A. Arboleya-Arboleya, J. Laviada, F. Las-Heras, N. Dolatsha, B. Grave, M. Sawaby, and A. Arbabian, "Ball grid array module with integrated shaped lens for 5G backhaul/fronthaul communications in F-band," *IEEE Trans. Antennas Propag.*, vol. 65, no. 12, pp. 6380–6394, Dec. 2017, doi: 10.1109/TAP.2017.2755439.

[4] A. Mozharovskiy, A. Artemenko, A. Sevastyanov, V. Ssorin, and R. Maslennikov, "Beam-steerable integrated lens antenna with waveguide feeding system for 71–76/81–86 GHz point-to-point applications," in *Proc. 10th Eur. Conf. Antennas Propag. (EuCAP)*, Apr. 2016, pp. 1–5, doi: 10.1109/EuCAP.2016.7481774.

[5] A. Artemenko, A. Mozharovskiy, A. Maltsev, R. Maslennikov, A. Sevastyanov, and V. Ssorin, "Experimental characterization of E-band two-dimensional electronically beam-steerable integrated lens antennas," *IEEE Antennas Wireless Propag. Lett.*, vol. 12, pp. 1188–1191, 2013, doi: 10.1109/LAWP.2013.2282212.

[6] A. Artemenko, A. Maltsev, A. Mozharovskiy, A. Sevastyanov, V. Ssorin, and R. Maslennikov, "Millimeter-wave electronically steerable integrated lens antennas for WLAN/WPAN applications," *IEEE Trans. Antennas Propag.*, vol. 61, no. 4, pp. 1665–1671, Apr. 2013, doi: 10.1109/TAP.2012.2232266.

[7] N. Chudpooti, S. Praesomboon, N. Duangrit, N. Somjit, and P. Akkaraekthalin, "An X-band portable 3D-printed lens antenna with integrated waveguide feed for microwave imaging," in *Proc. Photon. Electromagn. Res. Symp. Spring (PIERS-Spring)*, Jun. 2019, pp. 487–492, doi: 10.1109/PIERS-Spring46901.2019.9017614.

[8] A. Vorobyov, J. R. Farserotu, and J.-D. Decotignie, "3D printed antennas for mm-wave sensing applications," in *Proc. 11th Int. Symp. Med. Inf. Commun. Technol. (ISMICT)*, Feb. 2017, pp. 23–26, doi: 10.1109/ISMICT.2017.7891759.

[9] E. Erfani, M. Niroo-Jazi, and S. Tatu, "A high-gain broadband gradient refractive index metasurface lens antenna," *IEEE Trans. Antennas. Propag.*, vol. 64, no. 5, pp. 1968–1973, May 2016, doi: 10.1109/TAP.2016.2526052.

[10] K. V. Hoel, S. Kristoffersen, M. Ignatenko, and D. Filipovic, "Half ellipsoid Luneburg GRIN dielectric lens loaded double ridged horn antenna," in *Proc. 12th Eur. Conf. Antennas Propag. (EuCAP)*, 2018, p. 164, doi: 10.1049/cp.2018.0523.

[11] J.-M. Poyanco, F. Pizarro, and E. Rajo-Iglesias, "3D-printed dielectric GRIN planar wideband lens antenna for 5G applications," in *Proc. 15th Eur. Conf. Antennas Propag. (EuCAP)*, Mar. 2021, pp. 1–4, doi: 10.23919/EuCAP51087.2021.9411342.

[12] K. V. Hoel, M. Ignatenko, S. Kristoffersen, E. Lier, and D. S. Filipovic, "3-D printed monolithic GRIN dielectric-loaded double-ridged horn antennas," *IEEE Trans. Antennas Propag.*, vol. 68, no. 1, pp. 533–539, Jan. 2020, doi: 10.1109/TAP.2019.2938563.

[13] X. Wang, Y. Cheng, and Y. Dong, "A wideband PCB-stacked air-filled Luneburg lens antenna for 5G millimeter-wave applications," *IEEE Antennas Wireless Propag. Lett.*, vol. 20, no. 3, pp. 327–331, Mar. 2021, doi: 10.1109/LAWP.2021.3049432.

[14] N. Garcia and J. Chisum, "High-efficiency, wideband GRIN lenses with intrinsically matched unit cells," *IEEE Trans. Antennas Propag.*, vol. 68, no. 8, pp. 5965–5977, Aug. 2020, doi: 10.1109/TAP.2020.2990289.

[15] M. Sedaghat, V. Nayyeri, M. Soleimani, and O. M. Ramahi, "New approaches to design and realization of dielectric GRIN flat lenses," in *Proc. 5th Int. Conf. Millimeter-Wave Terahertz Technol. (MMWaTT)*, Dec. 2018, pp. 49–53, doi: 10.1109/MMWaTT.2018.8661237.

[16] C. Mateo-Segura, A. Dyke, H. Dyke, S. Haq, and Y. Hao, "Flat Luneburg lens via transformation optics for directive antenna applications," *IEEE Trans. Antennas Propag.*, vol. 62, no. 4, pp. 1945–1953, Apr. 2014, doi: 10.1109/TAP.2014.2302004.

[17] Y. He and G. V. Eleftheriades, "Matched, low-loss, and wideband graded-index flat lenses for millimeter-wave applications," *IEEE Trans. Antennas Propag.*, vol. 66, no. 3, pp. 1114–1123, Mar. 2018, doi: 10.1109/TAP.2018.2790173.

[18] Y. He and G. V. Eleftheriades, "A highly-efficient flat graded-index dielectric lens for millimeter-wave application," in *Proc. IEEE Int. Symp. Antennas Propag. USNC/URSI Nat. Radio Sci. Meeting*, Jul. 2017, pp. 2655–2656, doi: 10.1109/APUSNCURSINRSM.2017.8073370.

[19] N. I. Landy, N. Kundtz, and D. R. Smith, "Designing three-dimensional transformation optical media using quasiconformal coordinate transformations," *Phys. Rev. Lett.*, vol. 105, no. 19, pp. 3–6, Nov. 2010, doi: 10.1103/PhysRevLett.105.193902.

[20] T. Driscoll, G. Lipworth, J. Hunt, N. Landy, N. Kundtz, D. N. Basov, and D. R. Smith, "Performance of a three dimensional transformation-optical-flattened Lüneburg lens," *Opt. Exp.*, vol. 20, no. 12, p. 13262, Jun. 2012, doi: 10.1364/oe.20.013262.

[21] Z. L. Mei, J. Bai, and T. J. Cui, "Gradient index metamaterials realized by drilling hole arrays," *J. Phys. D, Appl. Phys.*, vol. 43, no. 5, Feb. 2010, Art. no. 055404, doi: 10.1088/0022-3727/43/5/055404.

[22] A.-E. Mahmoud, W. Hong, Y. Zhang, and A. Kishk, "W-band mutlilayer perforated dielectric substrate lens," *IEEE Antennas Wireless Propag. Lett.*, vol. 13, pp. 734–737, 2014, doi: 10.1109/LAWP.2014.2316144.

[23] N. Zhang, W. X. Jiang, H. F. Ma, W. X. Tang, and T. J. Cui, "Compact high-performance lens antenna based on impedance-matching gradient-index metamaterials," *IEEE Trans. Antennas Propag.*, vol. 67, no. 2, pp. 1323–1328, Feb. 2019, doi: 10.1109/TAP.2018.2880115.

[24] P. Kadera, J. Sánchez-Pastor, A. Jiménez-Sáez, M. Schußler, J. Lacik, and R. Jakoby, "QCTO Luneburg lens-based retroreflective tag landmarks for mm-wave self-localization systems," in *Proc. IEEE-APS Topical Conf. Antennas Propag. Wireless Commun. (APWC)*, Aug. 2021, pp. 105–108, doi: 10.1109/APWC52648.2021.9539571.

[25] Y. Zhao, J. Weidenmueller, G. V. Bogel, A. Grabmaier, A. A. Abbas, K. Solbach, A. Jimenez-Saez, M. Schusler, and R. Jakoby, "2D metamaterial Luneburg lens for enhancing the RCS of chipless dielectric resonator tags," in *Proc. 2nd Int. Workshop Mobile Terahertz Syst. (IWMTS)*, Jul. 2019, p. 5, doi: 10.1109/IWMTS.2019.8823784.

[26] F. Fan, M. Cai, J. Zhang, Z. Yan, and J. Wu, "Wideband low-profile Luneburg lens based on a glide-symmetric metasurface," *IEEE Access*, vol. 8, pp. 85698–85705, 2020, doi: 10.1109/ACCESS.2020.2992653.

[27] H. Lu, Z. Liu, Y. Zhang, K. Pang, and Y. Liu, "Partial Maxwell fish-eye lens inspired by the Gutman lens and Eaton lens for wide-angle beam scanning," *Opt. Exp.*, vol. 29, no. 15, p. 24194, Jul. 2021, doi: 10.1364/oe.426539.

[28] J. Ruiz-García, E. Martini, C. Della Giovampaola, D. González-Ovejero, and S. Maci, "Reflecting Luneburg lenses," *IEEE Trans. Antennas Propag.*, vol. 69, no. 7, pp. 3924–3935, Jul. 2021, doi: 10.1109/TAP.2020.3044668.

[29] N. J. Fonseca and O. Quevedo-Teruel, "Compact parallel plate waveguide geodesic lens for line sources with wide scanning range," in *Proc. 38th ESA Antenna Workshop Innov. Antenna Syst. Technol. Future Space Missions*, Oct. 2017, pp. 1–6.

[30] Q. Liao, N. J. G. Fonseca, and O. Quevedo-Teruel, "Compact multibeam fully metallic geodesic Luneburg lens antenna based on non-Euclidean transformation optics," *IEEE Trans. Antennas Propag.*, vol. 66, no. 12, pp. 7383–7388, Dec. 2018, doi: 10.1109/TAP.2018.2872766.

[31] N. J. G. Fonseca, "Experimental validation of a water drop geodesic lens design in Ka-band," in *Proc. 40th ESA Antenna Workshop Antenna Develop. Terr. Small-Space Platforms*, Oct. 2019, pp. 1–6.

[32] N. J. G. Fonseca, Q. Liao, and O. Quevedo-Teruel, "Equivalent planar lens ray-tracing model to design modulated geodesic lenses using non-Euclidean transformation optics," *IEEE Trans. Antennas Propag.*, vol. 68, no. 5, pp. 3410–3422, May 2020.

[33] K. Liu, S. Yang, S. Qu, Y. Chen, M. Huang, and J. Hu, "A low-profile wide-scanning fully metallic lens antenna for 5G communication," *Int. J. RF Microw. Comput.-Aided Eng.*, vol. 31, no. 5, pp. 1–8, May 2021, doi: 10.1002/mmce.22584.

[34] N. J. G. Fonseca, Q. Liao, and O. Quevedo-Teruel, "Compact parallel-plate waveguide half-Luneburg geodesic lens in the Ka-band," *IET Microw., Antennas Propag.*, vol. 15, no. 2, pp. 123–130, Feb. 2021, doi: 10.1049/mia2.12028.

[35] J. Tak, D.-G. Kang, and J. Choi, "A lightweight waveguide horn antenna made via 3D printing and conductive spray coating," *Microw. Opt. Technol. Lett.*, vol. 59, no. 3, pp. 727–729, Mar. 2017.

[36] S. Alkaraki, Y. Gao, M. O. M. Torrico, S. Stremsdoerfer, E. Gayets, and C. Parini, "Performance comparison of simple and low cost metallization techniques for 3D printed antennas at 10 GHz and 30 GHz," *IEEE Access*, vol. 6, pp. 64261–64269, 2018.

[37] K. Vieira Hoel, S. Kristoffersen, J. Moen, K. G. Kjelgård, and T. S. Lande, "Broadband antenna design using different 3D printing technologies and metallization processes," in *Proc. 10th Eur. Conf. Antennas Propag. (EuCAP)*, Apr. 2016, pp. 1–5.

[38] A. Romani, A. Mantelli, P. Tralli, S. Turri, M. Levi, and R. Suriano, "Metallization of thermoplastic polymers and composites 3D printed by fused filament fabrication," *Technologies*, vol. 9, no. 3, p. 49, Jul. 2021.

[39] R. Colella, F. P. Chietera, and L. Catarinucci, "Yagi-uda antenna with fully 3D-printed bow-tie elements," in *Proc. IEEE Microw. Theory Techn. Wireless Commun. (MTTW)*, vol. 1, Oct. 2020, pp. 62–66, doi: 10.1109/MTTW51045.2020.9245029.

[40] C. Prakash, P. Senthil, and T. Sathies, "Fused deposition modeling fabricated PLA dielectric substrate for microstrip patch antenna," *Mater. Today: Proc.*, vol. 39, pp. 533–537, 2020, doi: 10.1016/j.matpr.2020.08.258.

[41] *Rogers Web Site*. Accessed: Sep. 4, 2022. [Online]. Available: https://www.rogerscorp.com/advanced-electronics-solutions/radix-printable-dielectric

[42] *3DCeram Web Site*. Accessed: Sep. 4, 2022. [Online]. Available: https://3dceram.com/ceramics/

[43] *Carbon3D Web Site*. Accessed: Sep. 4, 2022. [Online]. Available: https://docs.carbon3d.com/files/technical-data-sheets/tds_carbon_epx-82.pdf?_ga=2.74040978.1443108774.1661773425-1662361352.1660915121

[44] K. Lomakin, M. Sippel, K. Helmreich, and G. Gold, "Design and analysis of 3D printed slotted waveguides for D-band using stereolithography and electroless silver plating," in *IEEE MTT-S Int. Microw. Symp. Dig.*, Aug. 2020, pp. 177–180, doi: 10.1109/IMS30576.2020.9223819.

[45] Y. Li, C. Wang, H. Yuan, N. Liu, H. Zhao, and X. Li, "A 5G MIMO antenna manufactured by 3-D printing method," *IEEE Antennas Wireless Propag. Lett.*, vol. 16, pp. 657–660, 2017, doi: 10.1109/LAWP.2016.2596297.

[46] G. Cung, T. Spence, and P. Borodulin, "Enabling broadband, highly integrated phased array radiating elements through additive manufacturing," in *Proc. IEEE Int. Symp. Phased Array Syst. Technol. (PAST)*, Oct. 2016, pp. 1–9, doi: 10.1109/ARRAY.2016.7832632.

[47] Y. Zhu, J. Li, and G.-L. Huang, "A lightweight 3-D printed dual-band high-gain slotted spherical antenna," *IEEE Antennas Wireless Propag. Lett.*, vol. 19, no. 4, pp. 552–556, Apr. 2020, doi: 10.1109/LAWP.2020.2971836.

[48] Á. Palomares-Caballero, A. Alex-Amor, J. Valenzuela-Valdés, and P. Padilla, "Millimeter-wave 3-D-printed antenna array based on gap-waveguide technology and split E-plane waveguide," *IEEE Trans. Antennas Propag.*, vol. 69, no. 1, pp. 164–172, Jan. 2021, doi: 10.1109/TAP.2020.3008620.

[49] *HP Web Site*. Accessed: Sep. 1, 2022. [Online]. Available: https://www.hp.com/us-en/printers/3d-printers/products/multi-jet-technology.html

[50] K. Lomakin, T. Pavlenko, M. Sippel, G. Gold, K. Helmreich, M. Ankenbrand, N. Urban, and J. Franke, "Impact of surface roughness on 3D printed SLS horn antennas," in *Proc. 12th Eur. Conf. Antennas Propag. (EuCAP)*, Apr. 2018, pp. 1–4, doi: 10.1049/cp.2018.1235.

[51] M. Ferrando-Rocher, J. Ignacio Herranz-Herruzo, A. Valero-Nogueira, and B. Bernardo-Clemente, "Selective laser sintering manufacturing as a low cost alternative for flat-panel antennas in millimeter-wave bands," *IEEE Access*, vol. 9, pp. 45721–45729, 2021, doi: 10.1109/ACCESS.2021.3067637.

[52] W. Mark Dorsey, A. Stumme, K. M. Charipar, and N. A. Charipar, "3-D-printed circular array for Wimax base station," *IEEE Antennas Wireless Propag. Lett.*, vol. 18, no. 6, pp. 1159–1163, Jun. 2019, doi: 10.1109/LAWP.2019.2911354.

[53] B. Zhang, L. Wu, Y. Zhou, Y. Yang, H. Zhu, F. Cheng, Q. Chen, and K. Huang, "A K-band 3-D printed focal-shifted two-dimensional beam-scanning lens antenna with nonuniform feed," *IEEE Antennas Wireless Propag. Lett.*, vol. 18, no. 12, pp. 2721–2725, Dec. 2019, doi: 10.1109/LAWP.2019.2950264.

[54] B. Zhang, Z. Zhan, Y. Cao, H. Gulan, P. Linnér, J. Sun, T. Zwick, and H. Zirath, "Metallic 3-D printed antennas for millimeter- and submillimeter wave applications," *IEEE Trans. THz Sci. Technol.*, vol. 6, no. 4, pp. 592–600, Jul. 2016, doi: 10.1109/TTHZ.2016.2562508.

[55] R. G. Edwards, C. M. Norton, J. E. Campbell, and D. Schurig, "Effective conductivity of additive-manufactured metals for microwave feed components," *IEEE Access*, vol. 9, pp. 59979–59986, 2021, doi: 10.1109/ACCESS.2021.3071486.

[56] B. Zhang, L. Wu, Y. Zhou, Y. Yang, H. Zhu, F. Cheng, Q. Chen, and K. Huang, "A two-dimensional multibeam lens antenna for hydrologic radar application," *IEEE Antennas Wireless Propag. Lett.*, vol. 18, no. 12, pp. 2488–2492, Dec. 2019, doi: 10.1109/LAWP.2019.2940999.

[57] B. Zhang, Y. Guo, Q. Guo, L. Wu, K. B. Ng, H. Wong, Y. Zhou, and K. Huang, "Dielectric and metallic jointly 3D-printed mmWave hyperbolic lens antenna," *IET Microw., Antennas Propag.*, vol. 13, no. 11, pp. 1934–1939, Sep. 2019, doi: 10.1049/iet-map.2018.6151.

[58] S. Zhang, R. K. Arya, S. Pandey, Y. Vardaxoglou, W. Whittow, and R. Mittraj, "3D-printed planar graded index lenses," *IET Microw., Antennas Propag.*, vol. 10, no. 13, pp. 1411–1419, 2016, doi: 10.1049/iet-map.2016.0013.

[59] J. Chen, Y. Zhao, L. Xing, Z. He, and L. Sun, "Broadband bifunctional Luneburg–Fisheye lens based on anisotropic metasurface," *Sci. Rep.*, vol. 10, no. 1, pp. 1–12, Nov. 2020, doi: 10.1038/s41598-020-77270-0.

[60] H. Saghlatoon, M. M. Honari, S. Aslanzadeh, and R. Mirzavand, "Electrically-small Luneburg lens for antenna gain enhancement using new 3D printing filling technique," *AEU Int. J. Electron. Commun.*, vol. 124, Sep. 2020, Art. no. 153352, doi: 10.1016/j.aeue.2020.153352.

[61] I. Grigoriev, I. Munina, and D. Zelenchuk, "3D printed Ku band cylindrical Luneburg lens," *J. Phys., Conf.*, vol. 2015, no. 1, Nov. 2021, Art. no. 012095, doi: 10.1088/1742-6596/2015/1/012095.

[62] R. K. Luneburg, *Mathematical Theory of Optics*. Berkeley, CA, USA: University of California Press, 1964, doi: 10.1525/9780520328266.

[63] O. Björkqvist, O. Dahlberg, and O. Quevedo-Teruel, "Additive manufactured three dimensional Luneburg lens for satellite communications," in *Proc. 13th Eur. Conf. Antennas Propag. (EuCAP)*, Apr. 2019, pp. 1–4.

[64] S. Biswas, A. Lu, Z. Larimore, P. Parsons, A. Good, N. Hudak, B. Garrett, J. Suarez, and M. S. Mirotznik, "Realization of modified Luneburg lens antenna using quasi-conformal transformation optics and additive manufacturing," *Microw. Opt. Technol. Lett.*, vol. 61, no. 4, pp. 1022–1029, Apr. 2019, doi: 10.1002/mop.31696.

[65] J. Budhu, Y. Rahmat-Samii, R. E. Hodges, D. C. Hofmann, D. F. Ruffatto, and K. C. Carpenter, "Three-dimensionally printed, shaped, engineered material inhomogeneous lens antennas for next-generation spaceborne weather radar systems," *IEEE Antennas Wireless Propag. Lett.*, vol. 17, no. 11, pp. 2080–2084, Nov. 2018, doi: 10.1109/LAWP.2018.2848263

[66] O. Bjorkqvist, O. Zetterstrom, and O. Quevedo-Teruel, "Additive manufactured dielectric Gutman lens," *Electron. Lett.*, vol. 55, no. 25, pp. 1318–1320, Dec. 2019, doi: 10.1049/el.2019.2483.

[67] S. Zhang, D. Cadman, W. Whittow, and J. C. Vardaxoglou, "Enabling extrusion based additive manufacturing for RF applications: Challenges and opportunities," in *Proc. 12th Eur. Conf. Antennas Propag. (EuCAP)*, 2018, no. CP741, p. 5, doi: 10.1049/cp.2018.0973.

[68] S. Zhang, D. Cadman, J. C. Vardaxoglou, R. Mittra, and W. Whittow, "Enabling additive manufacturing for microwave and Mm-wave components fabrication," in *Proc. Int. Conf. Microw. Millim. Wave Technol. (ICMMT)*, 2019 pp. 15–17, doi: 10.1109/ICMMT45702.2019.8992908.

[69] *Preperm Web Site*. Accessed: Sep. 4, 2022. [Online]. Available: https://www.preperm.com/products/raw-materials

[70] S. Zhang, P. Liu, and W. Whittow, "Design and fabrication of 3-D-printed high-gain broadband Fresnel zone lens using hybrid groove-perforation method for millimeter-wave applications," *IEEE Antennas Wireless Propag. Lett.*, vol. 21, no. 1, pp. 34–38, Jan. 2022, doi: 10.1109/LAWP.2021.3116459.

[71] J. M. Monkevich and G. Peter Le Sage, "Design and fabrication of a custom-dielectric Fresnel multi-zone plate lens antenna using additive manufacturing techniques," *IEEE Access*, vol. 7, pp. 61452–61460, 2019, doi: 10.1109/ACCESS.2019.2916077.

[72] J. M. Poyanco, F. Pizarro, and E. Rajo-Iglesias, "3D-printing for transformation optics in electromagnetic high-frequency lens applications," *Materials*, vol. 13, no. 12, pp. 1–11, 2020, doi: 10.3390/ma13122700.

[73] H. Giddens and Y. Hao, "Multibeam graded dielectric lens antenna from multimaterial 3-D printing," *IEEE Trans. Antennas Propag.*, vol. 68, no. 9, pp. 6832–6837, Sep. 2020, doi: 10.1109/TAP.2020.2978949.

[74] C. Wang, J. Wu, and Y.-X. Guo, "A 3-D-printed wideband circularly polarized parallel-plate Luneburg lens antenna," *IEEE Trans. Antennas Propag.*, vol. 68, no. 6, pp. 4944–4949, Jun. 2020, doi: 10.1109/TAP.2019.2955222.

[75] M. Norooziarab, D. McCloskey, D. S. Kozlov, V. V. Kirillov, S. Bulja, F. Pivit, and P. Rulikowski, "Millimeter-wave 3D printed Luneburg lens antenna," in *Proc. IEEE Radio Antenna Days Indian Ocean (RADIO)*, Sep. 2019, pp. 12–13, 2019, doi: 10.23919/RADIO46463.2019.8968885.

[76] Y.-H. Lou, Y.-X. Zhu, G.-F. Fan, W. Lei, W.-Z. Lu, and X.-C. Wang, "Design of Ku-band flat Luneburg lens using ceramic 3-D printing," *IEEE Antennas Wireless Propag. Lett.*, vol. 20, no. 2, pp. 234–238, Feb. 2021, doi: 10.1109/LAWP.2020.3046489.

[77] G. Wu, Y. Zeng, K. F. Chan, S. Qu, and C. H. Chan, "3-D printed circularly polarized modified Fresnel lens operating at terahertz frequencies," *IEEE Trans. Antennas Propag.*, vol. 67, no. 7, pp. 4429–4437, Jul. 2019, doi: 10.1109/TAP.2019.2908110.

[78] M. Yin, X. Yong Tian, L. Ling Wu, and D. Chen Li, "All-dielectric three-dimensional broadband Eaton lens with large refractive index range," *Appl. Phys. Lett.*, vol. 104, no. 9, Mar. 2014, Art. no. 094101, doi: 10.1063/1.4867704.

[79] W. Shao and Q. Chen, "Performance analysis of an all-dielectric planar Mikaelian lens antenna for 1-D beam-steering application," *Opt. Exp.*, vol. 29, no. 18, p. 29202, Aug. 2021, doi: 10.1364/OE.438182.

[80] Y. Li and Q. Zhu, "Luneburg lens with extended flat focal surface for electronic scan applications," *Opt. Exp.*, vol. 24, no. 7, p. 7201, Apr. 2016, doi: 10.1364/oe.24.007201.

[81] S. Biswas and M. Mirotznik, "High gain, wide-angle QCTO-enabled modified Luneburg lens antenna with broadband anti-reflective layer," *Sci. Rep.*, vol. 10, no. 1, pp. 1–14, Jul. 2020, doi: 10.1038/s41598-020-69631-6.

[82] P. Kadera and J. Lacik, "Performance comparison of W-band Luneburg lens antenna: Additive versus subtractive manufacturing," in *Proc. 20th Int. Conf. Microw. Techn. (COMITE)*, Apr. 2021, pp. 1–6, doi: 10.1109/COMITE52242.2021.9419879.
[83] J. Chen, H. Chu, Y. Zhang, Y. Lai, M. Chen, and D. Fang, "Modified Luneburg lens for achromatic subdiffraction focusing and directional emission," *IEEE Trans. Antennas Propag.*, vol. 69, no. 11, pp. 7930–7934, Nov. 2021, doi: 10.1109/TAP.2021.3083843.
[84] G. McKerricher, D. Titterington, and A. Shamim, "A fully inkjet-printed 3-D honeycomb-inspired patch antenna," *IEEE Antennas Wireless Propag. Lett.*, vol. 15, pp. 544–547, 2015.
[85] M. F. Farooqui and A. Shamim, "3-D inkjet-printed helical antenna with integrated lens," *IEEE Antennas Wireless Propag. Lett.*, vol. 16, pp. 800–803, 2017, doi: 10.1109/LAWP.2016.2604497.
[86] M. Liang, W. R. Ng, K. Chang, K. Gbele, M. E. Gehm, and H. Xin, "A 3-D Luneburg lens antenna fabricated by polymer jetting rapid prototyping," *IEEE Trans. Antennas Propag.*, vol. 62, no. 4, pp. 1799–1807, Apr. 2014, doi: 10.1109/TAP.2013.2297165.
[87] Y. Cao and S. Yan, "A low-profile high-gain multi-beam antenna based on 3D-printed cylindrical Luneburg lens," *Microw. Opt. Technol. Lett.*, vol. 63, no. 7, pp. 1965–1971, Jul. 2021, doi: 10.1002/mop.32862.
[88] K. So, K. Luk, C. Chan, and K. Chan, "3D printed high gain complementary dipole/slot antenna array," *Appl. Sci.*, vol. 8, no. 8, p. 1410, Aug. 2018, doi: 10.3390/app8081410.
[89] Y. Li, L. Ge, M. Chen, Z. Zhang, Z. Li, and J. Wang, "Multibeam 3-D-printed Luneburg lens fed by magnetoelectric dipole antennas for millimeter-wave MIMO applications," *IEEE Trans. Antennas Propag*, vol. 67, no. 5, pp. 2923–2933, Feb. 2019, doi: 10.1109/TAP.2019.2899013.
[90] H. Yi, S.-W. Qu, K.-B. Ng, C. H. Chan, and X. Bai, "3-D printed millimeter-wave and terahertz lenses with fixed and frequency scanned beam," *IEEE Trans. Antennas Propag.*, vol. 64, no. 2, pp. 442–449, Feb. 2016, doi: 10.1109/TAP.2015.2505703.
[91] Z. Qu, S.-W. Qu, Z. Zhang, S. Yang, and C. Hou Chan, "Wide-angle scanning lens fed by small-scale antenna array for 5G in millimeter-wave band," *IEEE Trans. Antennas Propag.*, vol. 68, no. 5, pp. 3635–3643, May 2020, doi: 10.1109/TAP.2020.2967086.
[92] G. Du, M. Liang, R. A. Sabory-Garcia, C. Liu, and H. Xin, "3-D printing implementation of an X-band Eaton lens for beam deflection," *IEEE Antennas Wireless Propag. Lett.*, vol. 15, pp. 1487–1490, 2016, doi: 10.1109/LAWP.2015.2514181.
[93] Y. Oh, V. T. Bharambe, J. J. Adams, D. Negro, and E. MacDonald, "Design of a 3D printed gradient index lens using high permittivity ceramic," in *Proc. IEEE Int. Symp. Antennas Propag. North Amer. Radio Sci. Meeting*, Jul. 2020, pp. 1431–1432, doi: 10.1109/IEEECONF35879.2020.9330193.
[94] K. Liu, C. Zhao, S.-W. Qu, Y. Chen, J. Hu, and S. Yang, "A 3-D-printed multibeam spherical lens antenna with ultrawide-angle coverage," *IEEE Antennas Wireless Propag. Lett.*, vol. 20, no. 3, pp. 411–415, Mar. 2021, doi: 10.1109/LAWP.2021.3054042.
[95] J. Pourahmadazar and T. A. Denidni, "Towards millimeter-wavelength: Transmission-mode fresnel-zone plate lens antennas using plastic material porosity control in homogeneous medium," *Sci. Rep.*, vol. 8, no. 1, p. 5300, Mar. 2018, doi: 10.1038/s41598-018-23179-8.
[96] P. I. Deffenbaugh, R. C. Rumpf, and K. H. Church, "Broadband microwave frequency characterization of 3-D printed materials," *IEEE Trans. Compon., Packag., Manuf. Technol.*, vol. 3, no. 12, pp. 2147–2155, Dec. 2013, doi: 10.1109/TCPMT.2013.2273306.
[97] *Prusa3D Web Site*. Accessed: Dec. 15, 2022. [Online]. Available: https://www.prusa3d.com/product/original-prusa-i3-mk3s-kit-3/#Specs/
[98] *Ultimaker Web Site*. Accessed: Dec. 15, 2022. [Online]. Available: https://ultimaker.com/3d-printers/ultimaker-s5/
[99] *Anycubic Web Site*. Accessed: Dec. 15, 2022. [Online]. Available: https://www.anycubic.com/products/photon-mono-x-6k/
[100] *Formlabs Web Site*. Accessed: Dec. 15, 2022. [Online]. Available: https://formlabs.com/3d-printers/form-2/
[101] *HP Web Site*. Accessed: Dec. 15, 2022. [Online]. Available: https://www.hp.com/us-en/printers/3d-printers/products/multi-jet-fusion-4200.html
[102] *Proto3000 Web Site*. Accessed: Dec. 15, 2022. [Online]. Available: https://proto3000.com/service/3d-printing-services/technologies/polyjet/
[103] *Sharebot Web Site*. Accessed: Dec. 15, 2022. [Online]. Available: https://www.sharebot.it/en/printers/snowwhite-2/

IRINA MUNINA (Member, IEEE) received the B.Sc. and M.Sc. degrees in radio engineering, in 2009 and 2011, respectively, and the Ph.D. degree in antennas and microwave devices from Saint Petersburg Electrotechnical University "LETI," Saint Petersburg, Russia, in 2016.

From 2016 to 2022, she was a Research Fellow in projects supported by the Ministry of Education and Science of Russian Federation, the Russian Science Foundation, and industrial companies. From 2020 to 2022, she was an Associate Professor with the Department of Microelectronics and Radio Engineering, Saint Petersburg Electrotechnical University "LETI." Since 2022, she has been a Research Fellow with the Department of Mechanical, Manufacturing and Biomedical Engineering, Trinity College Dublin, Ireland. Her research interests include design of microwave devices, including antennas and antenna arrays, metamaterials, metasurfaces, beamformers, additive manufacturing for design of antennas, and antenna arrays.

IGOR GRIGORIEV (Member, IEEE) was born in Kirov, Russia, in 2000. He received the B.S. degree in radio engineering and telecommunications from Saint Petersburg Electrotechnical University "LETI," Saint Petersburg, Russia, in 2022.

His research interest includes antenna design, particularly design of lens antennas.

Mr. Grigoriev was a recipient of a scholarship of the Government of Saint Petersburg in the field of physical sciences named after Zh. I. Alferov.

GARRET O'DONNELL is currently an Associate Professor with the Department of Mechanical and Manufacturing Engineering, Trinity College Dublin, and a Former Graduate with the Dublin Institute of Technology, University of Dublin, and NUI Dublin. His research interests include advancing the scientific understanding underpinning advanced manufacturing technologies in sectors, such as medical devices, automotive, and aerospace sectors. The core focus of the research work is the characterization of measurable phenomena in materials processing spanning length scales and spanning domains from machining to energy and resource consumption at factory systems level.

DANIEL TRIMBLE has been an Assistant Professor with the Department of Mechanical, Manufacturing and Biomedical Engineering, Trinity College Dublin, Dublin, Ireland, since September 2015. He is also a Principal Investigator (PI) with the Science and Technology in Advanced Manufacturing (STAM) Research Group and the Additive Research Laboratory (ARL), Trinity College Dublin, a Research Scholar with The International Academy of Production Engineering (CIRP), and an Associate Investigator with the Advanced Materials and BioEngineering Research (AMBER) Centre. His main research interests include metal 3D printing, precision machining, and modeling manufacturing processes.